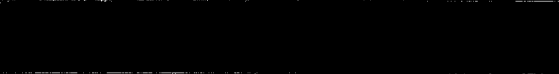# AN ABSTRACT OF THE THESIS OF

Jerry Ferdinand Cuderman   for the   Ph. D.   in   Physics
       (Name)   (Degree)   (Major)

Date thesis is presented   9-2-65

Title   ATOMIC EJECTION IN THE BEAM SPUTTERING OF NICKEL

    BY ARGON IONS, IN THE THRESHOLD TO 600 EV ENERGY

    RANGE

Abstract approved ▮▮▮▮▮▮▮▮▮▮▮▮▮▮▮

             (Major professor)

Using a low-energy, three stage, differentially pumped ion accelerator, similar to that used by Hagstrom for Auger electron ejection studies, permits, with the application of radiotracer methods, a new approach to the study of low energy sputtering.

The experimental approach consisted of pumping down the experimental tube to 10^{-9} torr, outgassing the target by electron bombardment, introducing argon into the system, and bombarding a Ni^{63} target for a time which is short compared to the time required for a monolayer of adsorbed gases to form at the existing residual partial pressure of adsorbable gases.

The target consisted of Ni^{63} plated on a cold-rolled nickel substrate. Heating the target above its recrystallization temperature produced an 80 percent oriented polycrystalline surface which approximated the (100) plane of a nickel single crystal. Mounting the

target so that its surface normal made an angle of 30° with respect to the incident beam direction and bombarding with argon ions produced the characteristic pattern for atoms sputtered from the close-packed directions or "chains" which terminate on the surface of a (100) plane.

The target was mounted inside a cylindrical collector, slightly behind center. The ion beam impinged on the target through a narrow slit in the collector. Sputtered atoms were collected on a removable molybdenum foil which lined the outer collector cylinder support. After each bombardment, the molybdenum foil was removed, cut into narrow strips, and then the strips were analyzed by placing them under a G-M counter.

The tracer technique permitted measuring the relative sputtering yields from individual crystallographic directions with respect to the angle of incidence of the ion beam. The method thus permitted a direct check on the Harrison-Magnuson theory of single-crystal sputtering thresholds. Contrary to their predictions, there was very little dependence of the threshold on angle of ion incidence with respect to a given chain direction. The observed sputtering yield curves flattened out or "saturated" at a much lower energy than those appearing in the literature. The saturation yield proved highly dependent on the angle of ion incidence. It appears, on the basis of the single direction yield curves, that the measurements appearing

in the literature represent a superposition of independent yield curves--from $\langle 110 \rangle$ and from $\langle 100 \rangle$ directions, respectively.

Reflection maxima of sputtered nickel atoms, which appeared behind the target on the collector surface, appear to be due to specular reflection from the primary maxima. A plot of the reflection ratios as a function of incident ion energy suggests that the specular reflection arises from resonance scattering from the interaction potential that the nickel atoms encounter at the molybdenum surface.

ATOMIC EJECTION IN THE BEAM SPUTTERING OF
NICKEL, BY ARGON IONS, IN THE THRESHOLD
TO 600 EV ENERGY RANGE

by

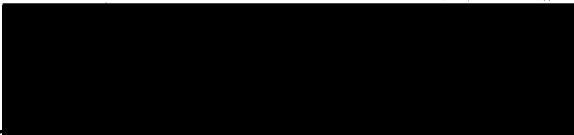JERRY FERDINAND CUDERMAN

A THESIS

submitted to

OREGON STATE UNIVERSITY

in partial fulfillment of
the requirements for the
degree of
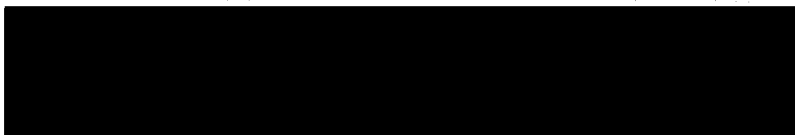
DOCTOR OF PHILOSOPHY

June 1966

APPROVED:

████████████████

Professor of Department of Physics

In Charge of Major

and

Acting Chairman of Department of Physics

████████████████

Dean of Graduate School

Date thesis is presented _9-2-65_

Typed by Eula Weathers

ACKNOWLEDGEMENT

TABLE OF CONTENTS

LIST OF FIGURES

LIST OF TABLES

ATOMIC EJECTION IN THE BEAM SPUTTERING OF NICKEL, BY ARGON IONS, IN THE THRESHOLD TO 600 EV ENERGY RANGE

I. INTRODUCTION

A. Definition of Sputtering

Studies of atomic ejection from surfaces under ion bombardment date back to the 1852 observation, by Grove (Wehner, 1961), that metal atoms are "sputtered" from the cathode in a glow discharge and deposited on the tube walls. The ejection process, which was thus labeled "sputtering," can be either chemical or physical sputtering, depending on the nature of the target and ions bombarding it.

Chemical sputtering occurs when the ions interact chemically with the surface atoms and the interaction energy which is given off causes, or contributes to, the ejection of a surface atom.

Physical sputtering, where no intermediate bond occurs, is the result of a direct momentum transfer from the bombarding ions to the atoms of the material being sputtered.

This study concerns the physical sputtering of nickel.

B. Experimental Requirements

a. Introduction

The essential requirements for a sputtering experiment include
(1) a suitable means for collecting and analyzing the distribution of
sputtered material, (2) a source of ions of well defined energy and
direction, and (3) a clean target surface.

b. Analysis of Sputtered Material

Means for measuring the amount of sputtered material include
the electrical detection of sputtered atoms by using a surface ioniza-
tion detector (limited to alkali metals), weighing, optical trans-
mission, and radioactive tracer methods.

c. Ion Sources

For bombarding ions having tens of kev incident energy,
various ion sources exist which provide ion current densities of
several ma/cm^2, thus assuring the maintenance of a clean target.
(Bombardment by noble gas ions is a common technique for pro-
ducing "clean" surfaces.)

In low energy experiments, below 1000 ev ion energy, ion
beams having current densities of several ma/cm^2 are not feasible.
Thus, most low energy studies use negative Langmuir probe targets

submerged in a low pressure plasma. This constrains the bombarding ions to be at least moderately well defined in energy and direction.

d. Target Cleanliness

Surface cleanliness is probably the most important parameter in a sputtering experiment. Very small amounts of occluded active gases, such as oxygen or nitrogen, have a large effect on the results of a sputtering experiment. Usually, studies of surfaces having even a sizable fraction of a monolayer of adsorbed gas or oxide layer yield little useful information with regard to the basic processes of sputtering. Indeed, surface cleanliness is probably the major difficulty in any surface physics experiment.

C. The Relationship of Sputtering to Other Surface Physics Experiments

Most surface physics experiments involve determination of electronic properties of materials near the surface. These include the classic experiments of electron ejection by positive ion bombardment (Hagstrom, 1953), photo electric emission experiments, and work in field ion microscopy and field emission microscopy.

Sputtering experiments promise to complement the electronic studies with important information on the binding energies of

surface atoms in different crystal planes.

Recent low energy electron diffraction work--such as reported by Germer (1965), MacRae (1964), and others--lies somewhere between the electronic and sputtering areas; it provides information valuable to both. These experiments furnish quantitative information on the amount of adsorption of gases onto the various crystal surfaces, and, in addition, evaluate "sticking probabilities" for different gases as a function of material and crystal orientation. The low energy electron diffraction experiments have done much to define such relative terms as "monolayer" and "surface cleanliness" more exactly.

D. Summary of Experimental Studies in Sputtering

Sputtering experiments, dated prior to 1940, reveal few important details of the sputtering process. Most of them utilized the normal glow discharge for their source of ions. This immediately introduced a large uncertainty in the energy and momentum of the bombarding ions. In addition, since the pressure required for a normal glow discharge is at least 0.1 torr, the mean free path of the sputtered ions was necessarily much smaller than the tube dimensions. This resulted in sputtered atoms diffusing throughout the discharge, thereby precluding measurement of either yield per ion or distribution of sputtered material.

More recent investigations, notably by Wehner and co-workers, circumvent most of the glow discharge difficulties by utilizing thermionically augmented, low pressure plasmas which operate at pressures of the order of 10^{-3} to 10^{-4} torr. This pressure is low enough to allow the ions to have mean free paths much greater than the tube dimensions. Submerging the target into the plasma and biasing it as a negative Langmuir probe, it is argued, assures normal ion incidence. The Langmuir-Childs law, upon measurement of the dark sheath thickness, yields the incident ion energy. A screen, placed opposite the target, collects the sputtered atoms. Weighing techniques or optical transmission measurements are the usual methods of determining the yield (number of atoms sputtered per incident ion). These "Langmuir Probe" experiments have provided a large number of yield measurements for many materials. In addition, for most materials, the curve of yield versus energy is approximately linear below about 200 ev. By extrapolating the yield curve to zero yield, these studies also provide an estimate of the threshold energy.

While one would perhaps like to define the sputtering threshold as the smallest ion energy required to eject an atom, experimentally, it is only possible to extrapolate the lowest yield points, on the linear portion of a yield versus energy curve, to zero yield. These lowest yield points usually correspond to ion energies of 40 ev or

50 ev. Some evidence exists that the yield decrease is not linear for bombarding ion energies below about 30 ev (Zdanuk and Wolsky, 1965); they indicate that there is a more or less asymptotic approach to the zero yield energy. However, most of the experimental literature designates the "sputtering threshold" as the point where the linear extrapolation crosses the energy axis. At present, this seems like the most practical approach.

Several reviews exist, which describe recent sputtering experiments and their results in detail. These include review articles in <u>Advances in Electronics</u>, by G. K. Wehner (1955), by Eric Kay (1962), and a Ph. D. thesis publication by M. Koedam (1961). The latter is included with the review articles for two reasons. First of all, he re-ran essentially all of the low energy experiments that had been done prior to 1961 by Wehner and others, using a slightly more sophisticated apparatus. Secondly, his discussion and bibliography of previous work appears as comprehensive as that of the review articles.

E. Shortcomings of the Langmuir Probe-Low Pressure Plasma Approach

Koedam (1961), in analyzing the distribution of ion energies in a Langmuir probe, showed that the half width energy spread is of the order of 10 ev for a 250 ev bombarding ion energy. Furthermore,

this energy spread is not constant but is a function of energy.

Estimation of sputtering thresholds has not been accurate enough to convince everyone that a threshold above the sublimation energy does indeed exist (Harrison and Magnuson, 1961). As stated, for most materials, the sputtering yield increases approximately linearly, with energy, up to about 400 ev, or more, and then levels off. It is difficult to measure yields below about 50 ev, because 40 V to 50 V potential is required to maintain a low pressure plasma. Also, the amount of material sputtered rapidly becomes too small to weigh, at energies below 50 ev, for reasonable sputtering times. Thus, extrapolation of the linear part of the yield curve, from above 40 ev to 50 ev, to zero yield gives the threshold energy values appearing in the literature.

As indicated, a high current density, of the order of several ma/cm^2, occurring in the low pressure plasmas, assures clean surface conditions. Under these conditions, material sputters so rapidly that partial pressures of active gases present in the plasma do not have time to build up to a monolayer on the target surface. However, the high current density, at higher energies in particular, causes heating of the target. The effect of temperature does not generally seem to be large, but it remains to be fully evaluated. It seems desirable to maintain the target at constant temperature for all points on the yield versus energy curve.

A large part of the data on sputtering is of a qualitative nature, consisting of photographs of sputtering patterns from single and polycrystals. The methods of measurement are not readily amenable to give angular distributions of sputtered material. It seems at least as important to obtain the distribution of sputtered material as it is to measure the absolute yield.

F. Comments on Theoretical Development

The theoretical situation is roughly the same as that in the experimental realm. Some qualitative agreement exists between experiment and theory. Harrison and Magnuson (1961) have calculated polycrystalline thresholds which "agree" reasonable well with experimental values. Silsbee (1957) has proposed a focussing mechanism, described in Chapter V, which predicts the focussing of momentum in the directions of closest packing in a crystal. Reference to his model is used to qualitatively explain the presence of anisotropic sputtering from single crystals.

In general, the so called "thermal spike" theories of sputtering, also discussed in more detail in Chapter V, are discredited, at least for low ion energies, in favor of momentum transfer theories utilizing the "free particle lattice" model with loss mechanisms.

No satisfactory theory seems to exist for predicting yield as a function of energy.

There seems to be general agreement that too few quantitative data exist to make possible more than a qualitative comparison between theory and experiment. On the other hand, present theory does not seem to adequately explain the quantitative data that do appear in the literature.

G. Proposed Program for Beam Sputtering, at Low Energies, Under Clean Surface Conditions

In the Langmuir probe studies cited, the high density ion bombardment sputters gas atoms off the surface as fast as they arrive. An alternate approach, eliminating most of the objections to recent techniques, is to bombard the target with a very low intensity ion beam in a clean system. The program proposed requires reduction of the partial pressure of adsorbable gases to such a low level that only a small fraction of a monolayer has time to occlude onto the target, during the course of an experiment, after initial outgassing.

It is possible to build a device which produces a 10^{-10} amp ion current at energies ranging from a few electron volts to 2000 electron volts, and having an energy spread of less than 1 ev at any given energy. Hagstrom (1953) described such an instrument for use in electron ejection experiments. Since the surface conditions required in sputtering are identical to those for electron ejection studies, Hagstrom's tube seems to eliminate all the difficulties encountered

in recent sputtering data. However, there is a new difficulty. With only 10^{-10} amp ion current, the amount of material sputtered, at 100 ev energy, is of the order of 10^{-9} gm/hr. However, this rate is sufficient to allow analysis of sputtered deposits by using radioactive tracer techniques, provided the specific activity of the sputtered atoms is high enough.

A survey of the Oak Ridge Isotopes Catalog (1963) indicated Nickel 63 as the most feasible isotope for this experiment.

The ensuing pages describe, in detail, the design of an experimental tube similar to Hagstrom's, the required supporting systems, the experimental techniques, and the results of the proposed program.

II. APPARATUS

A. Experimental Tube

a. General Description

The source of bombarding ions for the experiment was a three

stage, differentially pumped tube consisting of (1) an ion chamber

and extracting ion lenses, (2) accelerating and decelerating ion

lenses, and (3) the target-collector assembly. This tube is an

adaptation of the instrument used by Hagstrom for Auger electron

experiments (cited in Chapter I).

Figure 1 schematically indicates the basic tube design for the

first two stages; Figure 2 is a schematic of the target-collector

assembly. It should be noted that Stage I includes the ion chamber

and extracting lenses; Stage II contains the accelerating-decelerat-

ing lenses; and Stage III contains the target-collector assembly.

b. Ion Chamber and Extracting Lenses

Electrons from the filament (Figure 1, A), on impact with gas

ions introduced directly into the ion chamber (Figure 1, D), produce

ions and then proceed to the collector (Figure 1, F). Maintaining

of the electron collector below the second ionization potential en-

sures singly charged ions. A 150 gauss magnet (Figure 1, E),

Note: The designation X_{12} refers to a pair of parallel electrodes X_1 and X_2 taken as a unit.
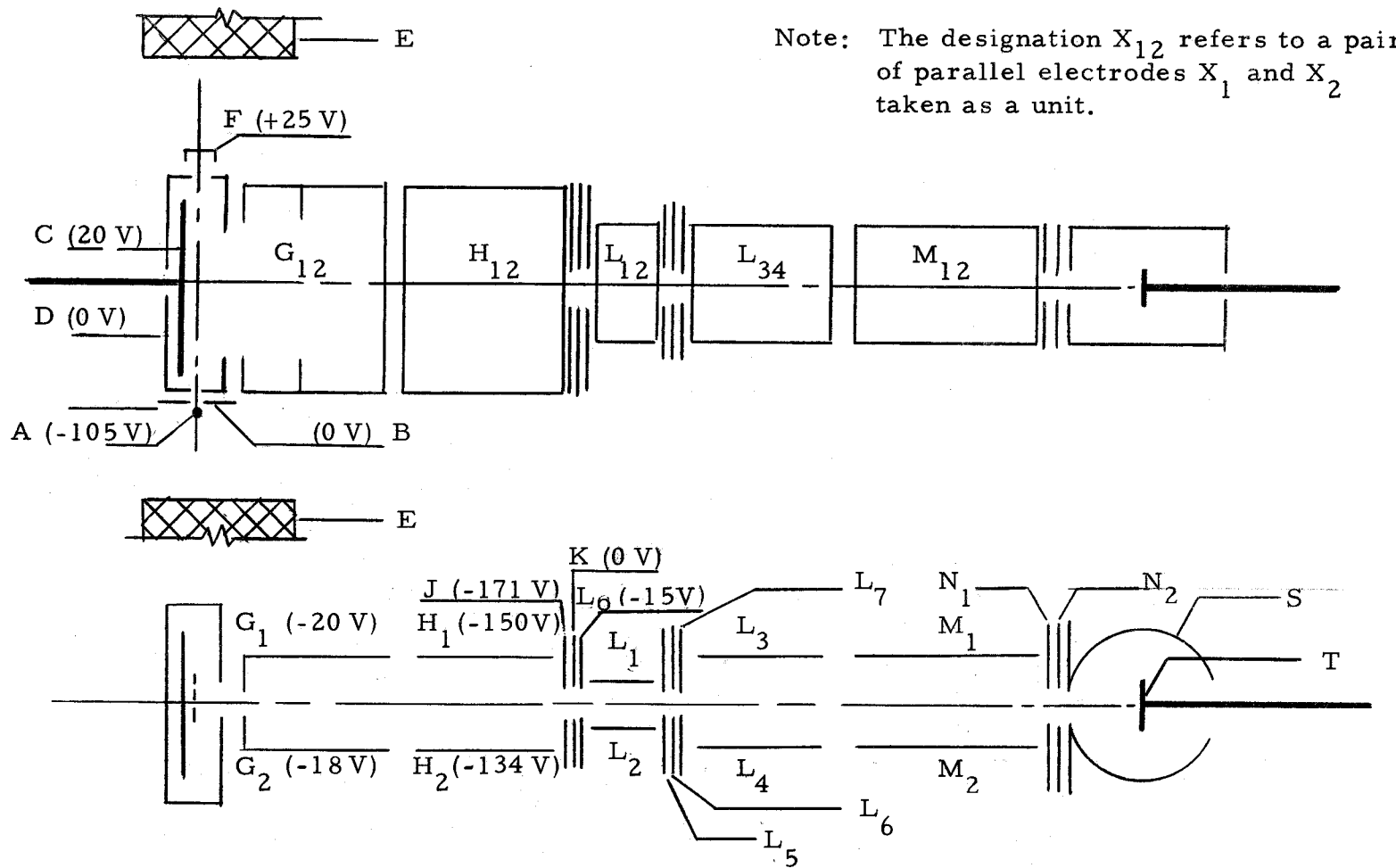
Figure 1. Experimental tube schematic.

A

B

Top View

A   A

S   G   C   E   D   F   B

Glass Insulator

Section A-A

Filaments
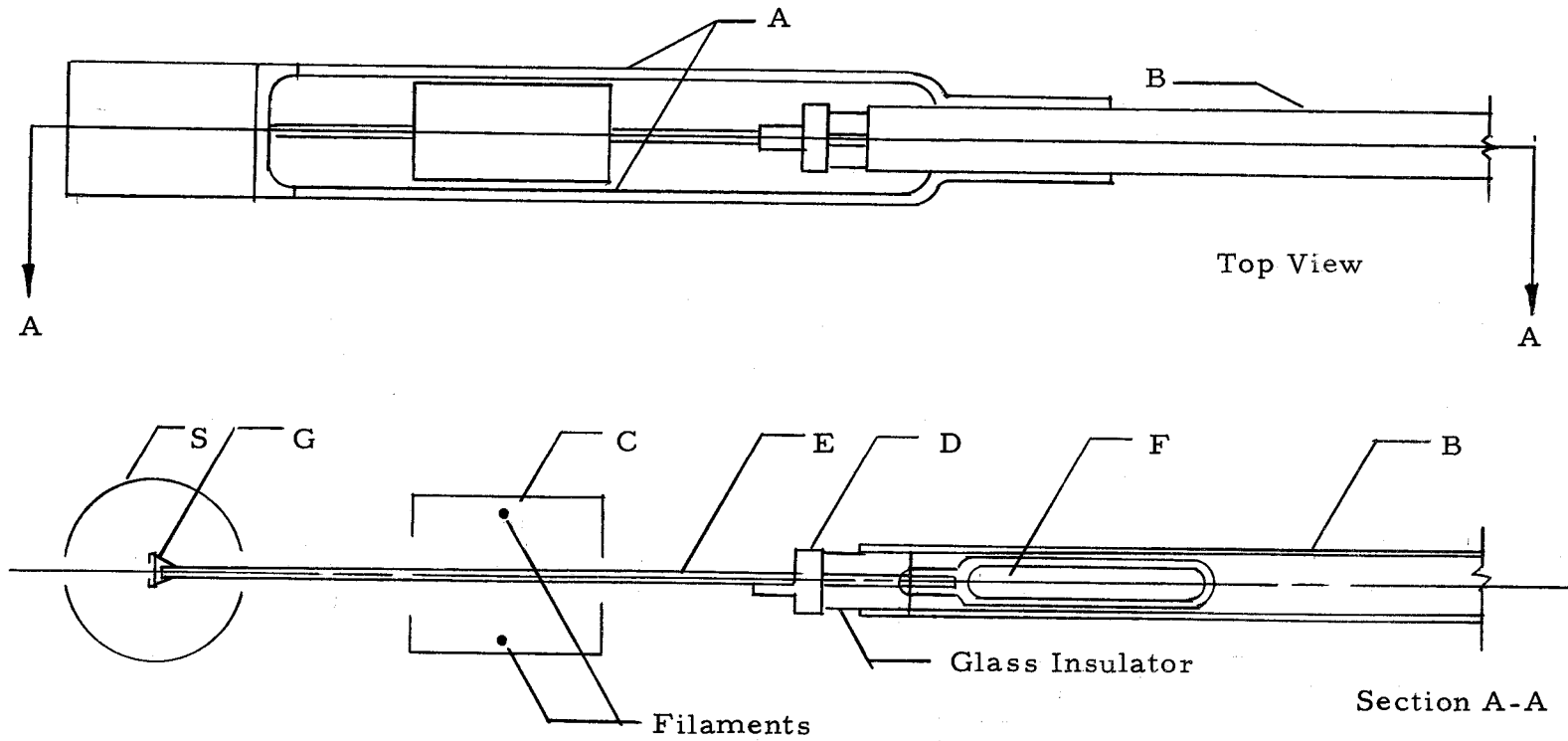
Figure 2.   Target-collector assembly schematic.

placed with the field lines parallel to the electron beam, increases

the ionization path and assists in focussing the electron beam. The

field of the repeller plate (Figure 1, C) forces the ions formed in

the ion chamber into the G-H lens system (Figure 1, G_{12}; H_{12})

which, in turn, focuses and accelerates them toward the $J-K-L_0$

apertures (Figure 1, $J-K-L_0$).

The potentials indicated in Figure 1 for Stage I elements re-

mained the same for all experimental runs.

c. Accelerating and Decelerating Lenses

The Stage II electrodes regulate the energies of ions delivered

to the target from several ev to about 100 ev, when used as a decel-

erating system, and from about 100 ev to 1000 ev, or more, when

used as an accelerating lens.

The $L_0-L_1-L_2$ aperture-cylinder lens (Figure 1, $L_0-L_1-L_2$)

reduces the angular spread of the beam as it comes out of the

$J-K-L_0$ aperture system.

The $L_5-L_6-L_7$ aperture system (Figure 1, $L_5-L_6-L_7$) stops

down the beam sufficiently to prevent ions from hitting any other

electrode enroute to the target.

The L-M lens (Figure 1, L_{34}; M_{12}) and the N_1-N_2-S saddle

field aperture configuration (Figure 1, N_1-N_2-S) bring the beam to

final focus onto the target.

The required potential ratios for Stage II electrodes are

V_M / V_L = 4.6 or 1/4.6 (depending on whether the lens is used for

accelerating or decelerating ions), V_{N_1} / V_M = 2.2, and V_M / V_S = 1.

A complete discussion of the design considerations involved,

as well as the development program leading to the final design,

appears in Hagstrom's paper.

d. The Target-Collector Assembly

The target-collector assembly consists of a chassis frame-

work, outgassing chamber, and a moveable target support.

The chassis framework consists of a collector foil support

(Figure 2, S) connected by two 1/8 in. stainless steel rods (Figure

2, A) to a 3/8 in. I.D. steel tube (Figure 2, B). Onto this frame

fastens the outgassing chamber (Figure 2, C). The moveable target

support slides in the steel tube, guided by the contact support

(Figure 2, D).

The outgassing chamber consists of two 5 mil tungsten fila-

ments connected in parallel and enclosed in a tantalum box. The

purpose of the box is to prevent evaporated tungsten from coating

the insulators in Stage III.

The moveable target support is made up of a 50 mil tungsten

rod, (Figure 2, E) ground flat on one side to slide on the contact

support. One end of the tungsten rod is embedded in a graded glass

seal fastened to a pyrex capsule which contains an iron slug (Figure 2, F). The capsule, actuated by an external magnet, slides inside the stainless steel tube to move the attached target into the out-gassing chamber and back again to its normal position inside the collector. The target holder (Figure 2, G) consists of a piece of 5 mil tantalum, bent into a channel shape and spotwelded onto a nickel frame which in turn is spotwelded to the tungsten target support rod. The long side of the 1/8 in. by 3/8 in. target lies parallel to the exit slit from Stage II. Each lip of the target holder, into which the target slides, overlaps the bombarded side of the target by less than 1/64 in.

A "stop" in the stainless steel tube restricts the movement of the target assembly so that the filament is always behind the target during the outgassing operation. This prevents the target from acquiring a film of evaporated tungsten.

A 0.625 in. by 2.75 in. strip of 6 mil molybdenum, shaped to conform to the inside surface of the 0.94 in. I.D. collector support, serves to collect the sputtered material.

Only three external electrodes provide all of the required connections to the target collector assembly. One electrode con-nects to the slider contact support; it provides the target potential. The negative terminal of the outgassing filaments and the chassis framework connect to a common electrode. The positive end of the

filaments connects to the third electrode.

e. Lens Design Adaptations

During the development of the tube, Hagstrom built four dif-
ferent instruments which were variations of the same basic design.
To some extent, features of all four are incorporated into the tube
used for this experiment. The N_1-N_2-S configuration, as shown in
Figure 1, is that used in Hagstrom's Instrument III. The Stage II
configuration is that of Instrument II; it affords the greatest degree
of beam control.

All of the instruments except Instrument III used a mass
analyzer section between Stages I and II. However, Instrument III
did not have the L_0-L_1-L_2 elements in Stage II. Thus, since the
sequence in Instrument II, through the analyzer, was J-K(entrance)-
K(stop)-K(exit)-L_0, the K(stop) and K(exit) electrodes do not appear
in my version. This approach seems justified since the K(entrance)
and K(exit) conditions are substantially identical.

f. Construction

Figure 3 shows the complete experimental tube, while Figure
4 indicates the general construction used in Stage I and Stage II
electrode assemblies. A special fixture, which held the electrodes
in position, permitted spot welding of the various elements to the
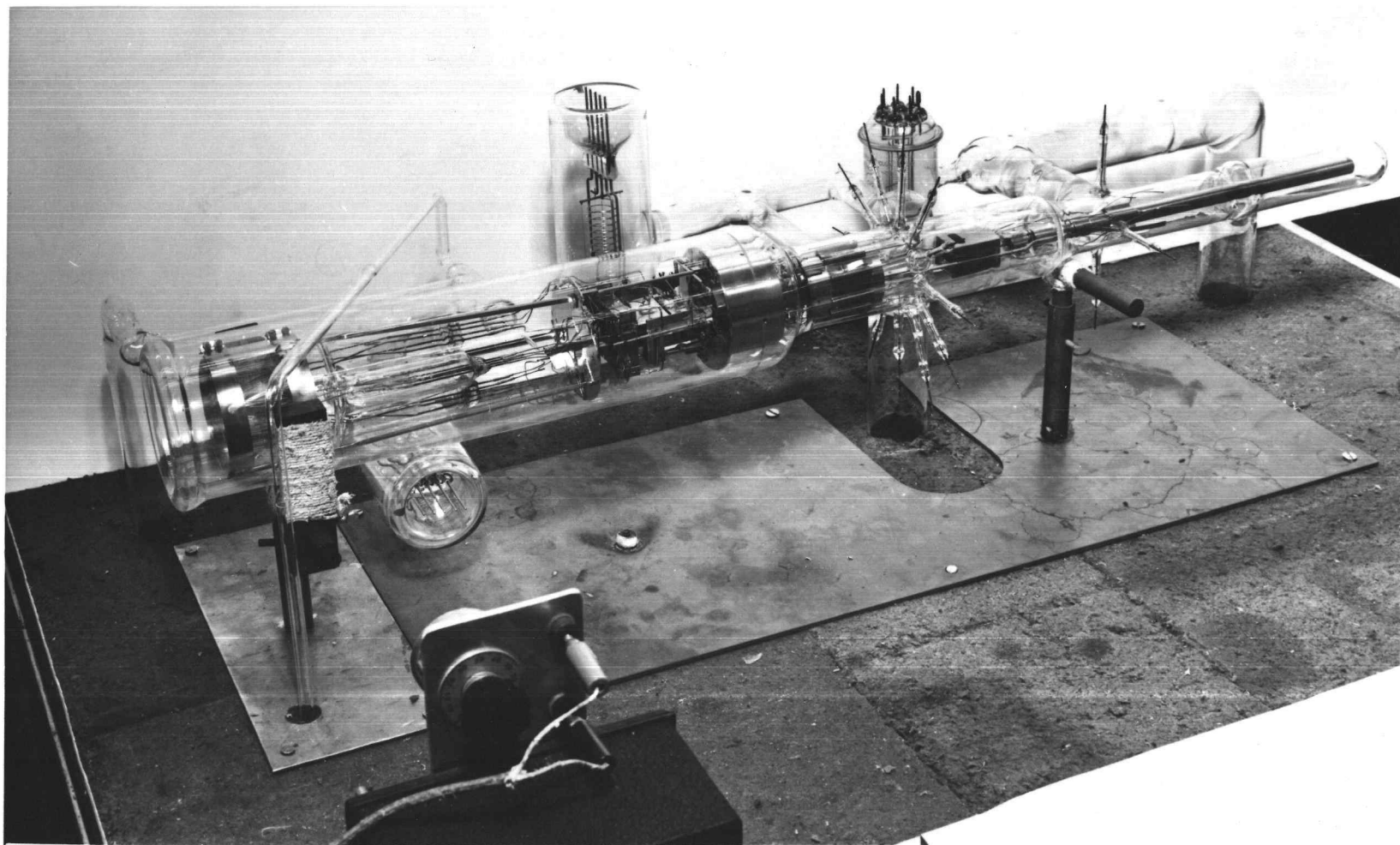
Figure 3. Experimental tube assembly.
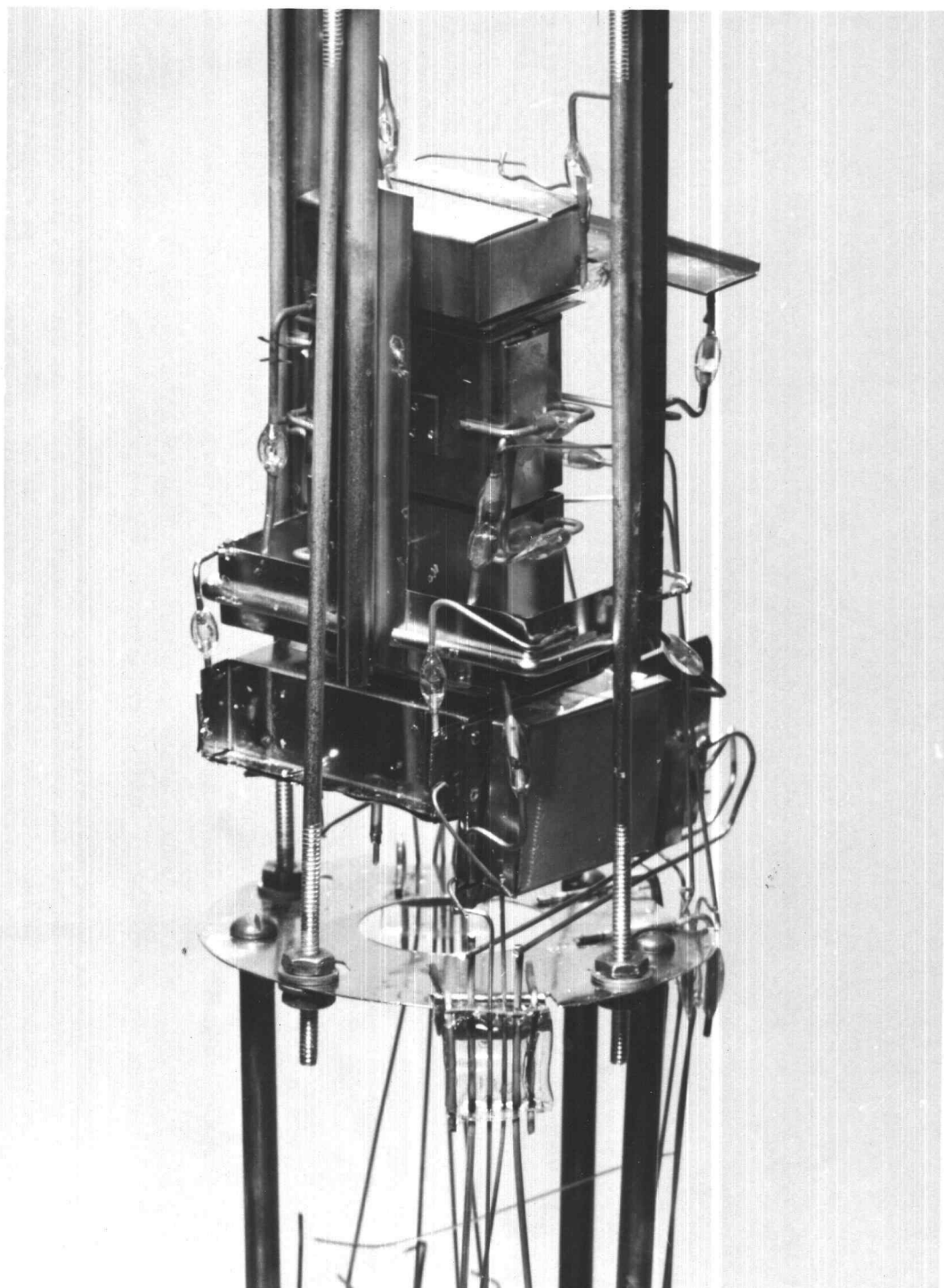
Figure 4. Stage I electrode assembly.

frame of each stage by way of an intermediate insulator. The glass
bead insulators which thus act as support members for the elec-
trodes, consist of two kovar wires fused into 7052 glass. The elec-
trode material is tantalum.

An important design modification of Hagstrom's tube is the all
glass envelope; it permits a much higher bakeout temperature than
Hagstrom's design which featured large metal to glass transitions
between successive stages. Figure 5 schematically shows the en-
velope design. As is seen, the tube itself acts as the primary sup-
port for the electrode assemblies. The three stages of the tube
envelope overlap and connect by previously annealed ring seals;
slits cut in the ends of the transition sections match up with elec-
trode assemblies on either side.

The first step in constructing the Stage II and Stage III envelope
sections consisted of placing the glass tubing on the lathe and closing
it off "square," at one end, with a torch. The next step was to hone
and polish the squared end on a lap. A high speed Dremel grinding
instrument was used to cut the slits in the polished faces. The
apertures sandwiching the glass slit between them fit flush on both
surfaces and were always chosen to be those which impressed the
smallest potential across the glass aperture. These precautions
minimized electrostatic effects due to the presence of dielectric
material in the lens system.
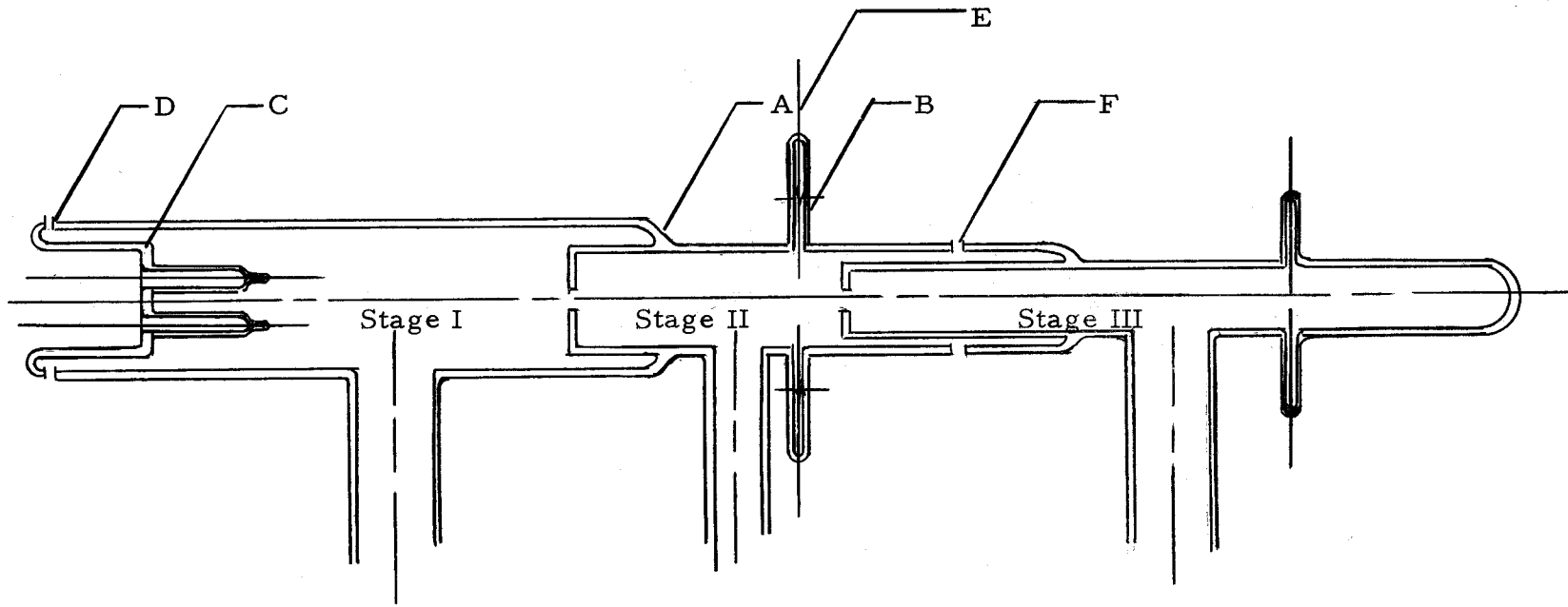
Figure 5.   Tube envelope schematic.

The final assembly began with the making of the Stage I to Stage II ring seal (Figure 5, A). Prior to this, glass stubs were installed around the Stage II section for attaching the lead-throughs (Figure 5, B). Annealing at 540°C, after these operations, relieved any strains which might have occurred. Completion of the Stage I assembly, by installing the Stage I electrodes, followed the annealing process. The Stage II envelope section extending into Stage I and the Stage I lead-through base (Figure 5, C) support the first stage electrode structure. Figure 5, D indicates the sealoff point for Stage I.

Next, spot welding of the lead-throughs to the Stage II electrodes followed visual alignment of Stage II with the Stage I exit slits and installation of lead-throughs (Figure 5, E).

The Stage III section, with a previously formed and annealed ring seal, was now cut to length and fused to Stage II at the point indicated by Figure 5, F. This completed the construction of the major sections of the tube, and installation onto the vacuum system followed.

The target-collector assembly slides into position in Stage III and spot welds to the three lead-throughs. This construction permits the sealing-off of Stage III into a test tube end which is easy to crack off for collector removal and permits maximum ease in resealing the tube.

Construction of the experimental tube covered a time span of about two years. Extensive testing of the Stage I electrode assembly, in a demountable system, enabled the development of a durable filament design and permitted checking out of the extraction lens system. No testing preceded permanent installation of the Stage II electrode assembly.

B. Vacuum System

Three 80 l/sec H.S. Martin mercury diffusion pumps connect to the respective stages of the experimental tube. The pumps were cold-trapped with liquid nitrogen both on the high vacuum and fore sides.

Two Cenco Hyvac-7 roughing pumps, vented to atmosphere, provide the fore vacuum; the first connects to the Stage I diffusion pump; the second connects to the Stage II and Stage III pumps.

A third Hyvac-7 purges the argon supply line to the ion chamber. The supply line, made of copper tubing, connects from the argon regulator to a needle valve, then to a break seal, to a Granville-Phillips high vacuum valve, and to the ion chamber, in that order. The Hyvac-7 connects to the supply line through a cold trap and high vacuum stopcock. The particular Granville-Phillips valve installed in the line was defective and therefore could not be closed off beyond 10^{-8} torr. The glass break seal, installed just

before the high vacuum valve, made it possible to completely isolate the experimental tube during bakeout and pumpdown.

Under dynamic conditions, the system produced a Stage I to Stage III differential pressure ratio of about 50.

Cooling water for the diffusion pumps flows from the tap through a solenoid valve then through a 25 ft length of garden hose to a pressure switch and manifold which distributes the water to the three diffusion pumps. The water exhausts from the diffusion pumps connect to a common exhaust manifold which then returns the water to the sink drain. A manual over-ride switch bypasses the pressure switch to permit starting of the system.

In the event of a sudden drop in water pressure, the pressure switch shuts off a bank of outlets which services the solenoid valve, the diffusion pump heaters, and the Simplytrol oven control units. Conversely, a shutoff of power shuts off the solenoid valve which then results in a pressure drop in the diffusion pump cooling system. On restoration of power, it is necessary to start the diffusion pumps and solenoid valve manually by switching on the over-ride switch for a few minutes.

C. Bakeout System

The bakeout system consists of a 900 watt capacity main oven and three trap ovens of 450 watts each. A squirrel-cage fan

installed in the main oven ensures a uniform temperature throughout the main oven. The trap ovens are small enough that fans are not necessary.

D. Instrumentation

a. Introduction

The basic instrumentation for the experiment was (1) the experimental tube power supply apparatus, (2) the oven controls, (3) the ion gauge controls, and (4) the collector analysis apparatus.

b. Experimental Tube Power Supply Apparatus

The experimental tube power supply apparatus consisted of three power supply units connected to a voltage divider, an Oregon Dual Power Supply, and filament current controls for the outgassing chamber and ion chamber filaments.

The three power supplies provided negative voltages from 0-450 volts to potentiometer controls 1-15, 0-300 volts to controls 16-24, and up to 1000 volts to potentiometers 25-30. It should be noted that the power supply to potentiometer controls 25-30 can provide up to 2000 volts. However, any potential over 1000 volts exceeds the rating of the potentiometers as installed. To permit operation at 1000 volts, 70 K bleeder resistors were installed

between the high voltage potentiometers and ground. A weakness in the voltage divider design became apparent when a "short" occurred in Stage I, about half way through the experimental runs. The "short" proved sporadic for several runs; continued attempts to run, prior to correcting the condition, resulted in burning out several of the potentiometers. A few of the potentiometers burned out while operating near their rated values (10 watts).

While the voltage divider arrangement proved generally adequate, a more heavy duty system, having individually fused potentiometers, would have been desirable. Figure 6 shows the voltage divider circuit.

Figure 7, Experimental Apparatus Installation, shows the voltage divider, centered in the relay rack at the right. The power supply at the bottom of the relay rack is the 2000 volt maximum unit; the one directly above it is the 0-300 volt supply. The 0-450 volt unit is behind the relay rack and does not appear in the photograph. The Oregon Dual Power Supply, directly below the voltage divider, provided the positive voltages required by elements C and F of the experimental tube (Figure 1, C, F).

Edison cells, connected to the laboratory from a central distribution panel, provided 12 volt power for the outgassing and ion chamber filaments. The rheostat and ammeter, at the extreme left, on top of the relay rack of Figure 7 controlled the power to the
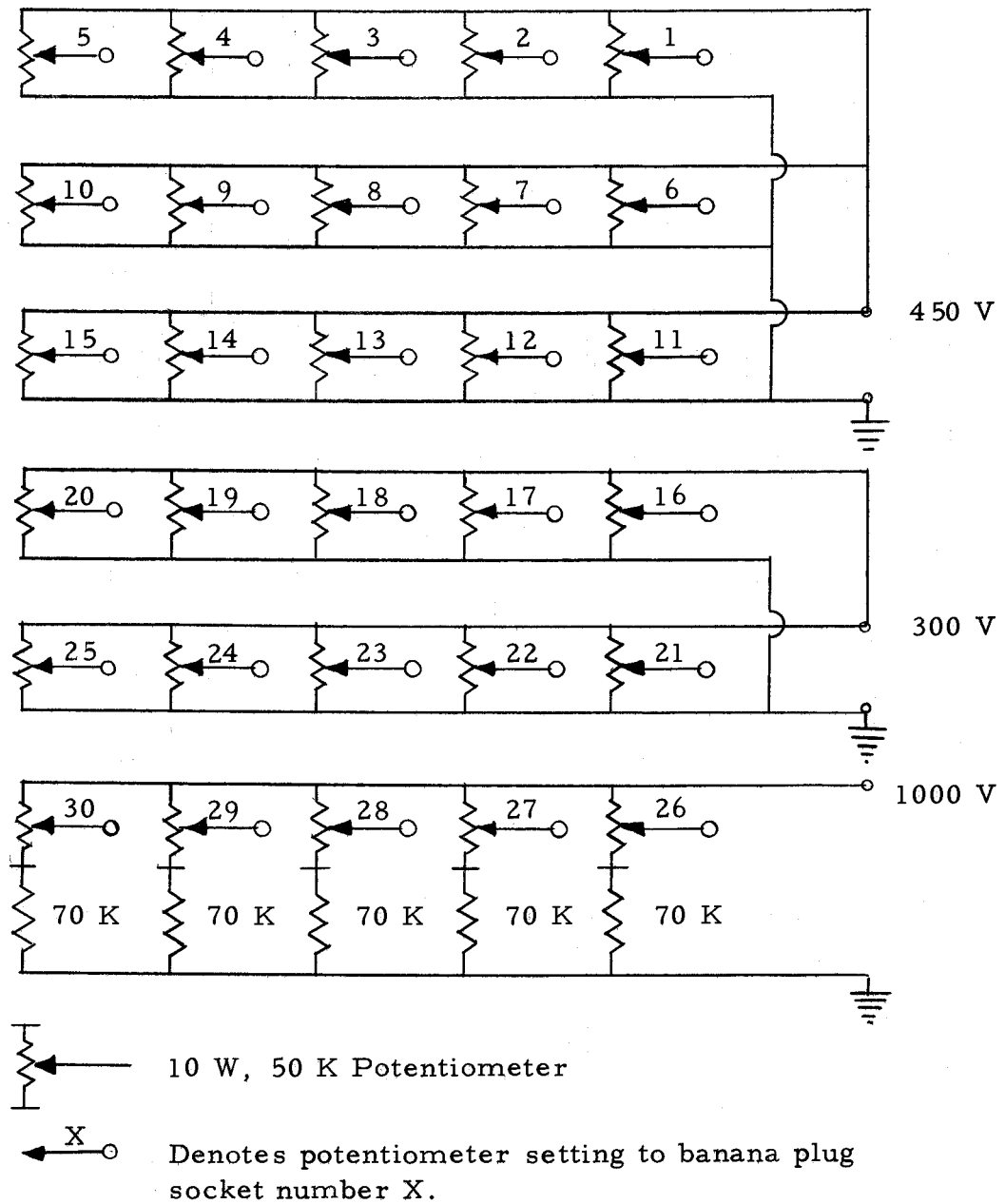
Figure 6. Voltage divider schematic.
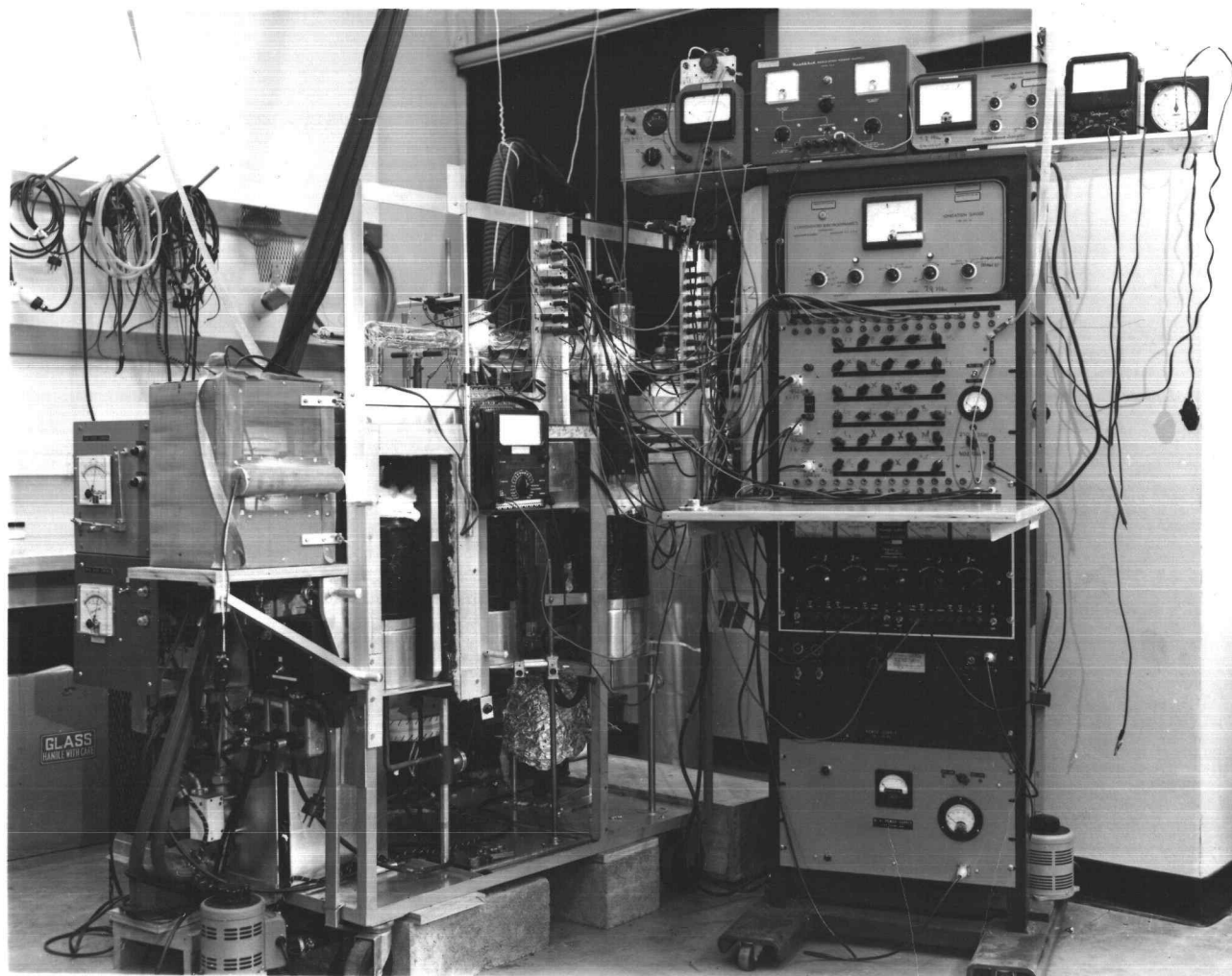
Figure 7. Experimental apparatus installation.

ion chamber filament; the unit next to it controlled the outgassing filaments. The Heathkit power supply biased the target during out-gassing.

The shielded instrument on the removeable shelf attached to the vacuum system frame, shown in Figure 7, is the Kiethly Model 600A electrometer which measured the ion current to the target. The electrometer was installed in the line from the voltage divider; this means that it "floated" at target potential. Initially, without shielding, stray currents made it impossible to operate the instru-ment below 10^{-9} amp; shielding of the electrometer, as shown, makes possible readings in the 10^{-11} amp range. An additional shielding screen, not shown, extended over the target end of the tube to enclose the target chamber electrodes. It was necessary to ground both the shielding screens and the voltage divider ground to water pipes. The screen over the dial of the electrometer made it difficult to read the instrument; a showcase light installed in front of the meter solved that problem.

As is shown in Figure 7, all lead wires from the relay rack and controls go to a readily demountable wiring harness frame which attached to the vacuum system frame. Pewee clip leads from the wiring harness connect to the Stage II and III tube electrodes. Spade connector leads connect to the Stage I elements. The wiring harness hangs, out of the way, on the relay rack during the bakeout cycle.

c. Oven Controls

The main oven has six separate elements controlled by individual toggle switches to permit increasing the heat input as needed. Each trap oven, except that for Stage I, has three separate elements and switches. Since a rheostat controls the Stage I trap oven power input, its elements were all tied in parallel initially.

Iron-Constantan thermocouples go from the main oven and trap ovens to the Symplytrol control units. A toggle switch on the Stage II unit permits cutting in the Stage I thermocouple, momentarily, to check the Stage I temperature.

When the temperature of an oven increases to a pre-set level, the Symplytrol opens the oven power relay which connects 115 volt line power to the oven elements. The reset cycle of the Symplytrol, after attaining a pre-set temperature, is one minute.

To prevent overloading circuits, each oven relay connects to a different 115 volt line circuit.

d. Ion Gauge Controls

Initially, three Bayard-Alpert type ion gauges monitored the pressure in the three respective chambers of the tube. However, the fringing fields from the magnetron magnet, which straddled the ion chamber, destroyed the accuracy of the Stage II reading. In

addition, the gauge interfered with optimal mounting of the magnet. Thus, it was removed.

A Cenco GIC-017 ion gauge and GIC-110A control, capable of measuring pressures into the 10^{-8} torr range, monitored the Stage I pressures. A Cenco GIC-001 ion gauge and GIC-100 control, capable of measuring pressures in the 10^{-11} torr range, indicated the Stage III pressure.

In addition, the Cenco GIC-100 gauge power supply provided two thermocouple gauge circuits and gauges for monitoring Stage I and Stage II-III forepump manifold pressures.

e. Collector Analysis Apparatus

The collector analysis apparatus included a Baird Atomic abacus scalar, a 1.4 mg/cm^2 thin window G-M tube and a 2 in. thick lead "doghouse" in which the tube and collector samples mounted.

The G-M tube fits into a hole in the top of a grooved sample holder in the doghouse. A 1/4 in. aluminum plate, which slips into the sample holder, fits flush against the window of the G-M tube. The 1/4 in. plate has a 1/8 in. by 1 in. groove across it, directly below the tube window. A slider, having a slot for holding a specimen of dimensions 1/8 in. by 1 in., slides in the groove. The slot,

while a section of the collector was being analyzed, centered direct-

ly below the G-M tube.

III. EXPERIMENTAL PROCEDURES

A. Target Preparation

The target was a piece of 1/8 in. by 3/8 in. by 8 mil cold rolled nickel foil onto which was plated nickel 63.

The source of Ni^{63} was the Isotopes Division of the Oak Ridge National Laboratory. Table I includes the Specifications given on the assay sheet which accompanied the isotope.

Table I. Isotope Specifications

Specification	Quantity or Description
Method of Production	$Ni^{62}(n, \gamma) Ni^{63}$ (Ni^{62} Enriched Target)
Type of Activity	Beta: 0.067 Mev, Gamma: None Other: None
Half Life	125 years
Amount Shipped	5 mc
Volume	3.9 ml
Nickel Concentration	0.11 mg/ml
Specific Activity	11,909 mc/gm
Chemical Form	$NiCl_2$ in HCl Solution
Normality	1.25 acid
Total Solids	0.75 mg/ml
Impurities	$Co^{60} < 0.001$ mc/ml
	$Co^{58} \sim 0.0000125$ mc/ml

It is noted that total solids add to 0.75 mg/ml of which nickel constitutes only 0.11 mg/ml. Correspondence with Oak Ridge National Laboratory revealed that the unknown solid is probably silicone oil; they advised that fuming with nitric acid removes it.

The literature provides no recipe for plating from very dilute $NiCl_2$ solutions. It does, however, in the directions for plating from standard solutions, provide some clues as to the important variables. These include buffering with boric acid, control of pH, and control of plating bath temperature (Creighton and Koehler, 1944).

Use of a special plating fixture ensured reproducible plating conditions. A 20 ml beaker containing the plating solution hung suspended in a 50 ml beaker filled with water. A small heating element, connected to a variac and located beneath the 50 ml water bath, controlled the plating solution temperature. A variable cathode-carbon anode spacing permitted tests to optimize the spacing.

A successful plating procedure developed out of experiments with simulated solutions. The most critical requirements for plating from the isotope solution proved to be a temperature of $70^{o}C$ and a pH of 6. The addition of NH_4OH regulated the pH. Universal pH Indicator paper was used to monitor the level. The addition of HBO_3 proved less critical; 0.01 mg/ml proved adequate. A plating

current density of 0.5 ma/cm^2 to 1 ma/cm^2 proved optimum with

a 1/2 in. cathode-anode spacing.

Successful plating of the target required 45 min at 0.68 ma.

Fuming with nitric acid to remove organic solids was not necessary.

Preparation of the nickel substrate by electrolytic polishing, in a

phosphoric acid bath, at 24 volts anode-cathode potential, followed

by a distilled water rinse, assured a clean plating surface.

B. Analysis of the Target

a. General Procedure

The cathode was a strip of nickel 3/8 in. wide by 1 in. long.

About 1/4 in. of this strip extended into the plating solution. Two

strips 1/8 in. wide were cut off the plated end of the cathode for

possible use as targets. Tests were run (1) to determine the activ-

ity by using successive layers of mylar between the target and

detector to determine the plating thickness and (2) to determine the

distribution of plated material on the target.

b. Determination of Plating Thickness

Analysis of the target, to determine plating thickness pro-

ceeded by placing the target 0.3 cm from a 1.4 mg/cm^2 window

G-M tube and measuring the count rate as a function of the number

of layers of 0.66 mg/cm^2 mylar interposed between the target and
detector. The count rate versus absorber thickness, plotted on
semi-log paper and extrapolated to zero thickness, gave an estimate
of the target activity. The smallest absorber thickness for which
the count rate was measured was 1.7 mg/cm^2, and the largest was
4.88 mg/cm^2. Drawing a "best straight line" through the points
and extrapolating to zero thickness gave a value of about 5 X 10^6
cpm (Counts Per Minute). Dead time and solid angle corrections,
as described in Bleuler and Goldsmith (1960), increased the value to
10^7 cpm. Correction for bremsstrahlung was necessary at the
lower count rates. This was done by subtracting the count rate
(less background) that resulted on placing a 0.020 in. aluminum
plate between the sample and detector.

The extrapolation to zero thickness extended over more than
one cycle of semi-log paper. There was no way to measure back-
scattering and reflection from the target and mylar layers. Thus,
this method, at best, only provides an estimate of the plating thick-
ness. It would have been desirable to measure the intensity of the
plating solution before and after plating using a fixed geometry
G-M counter. Unfortunately, this was not done. Comparison of the
depleted specimen with a second isotope, later obtained from Oak
Ridge, indicated that 24 percent of the nickel had plated out of the
original sample. The measured intensities of the two plated target

specimens were approximately equal. In addition, about the same activity appeared on both sides of each target. On this basis, the comparison test predicted that the activity of each side of the target should be about 0.3 mc, as compared with 0.02 mc given by the absorber method. In terms of mass plated, these values correspond to 2×10^{-6} gm and 25×10^{-6} gm respectively. Converting into "monolayers" yields about 30 and 300 respectively.

Visual inspection of the surface, with a 40 power microscope revealed a smooth continuous surface. A clean line of demarcation appeared between plated and unplated material. Since thin films of less than 100 monolayers are generally quite transparent, the 30 monolayer figure appears to represent a conservative lower bound.

As pointed out in Chapter I, G, the expected sputtering yield if of the order of 10^{-9} gm/hr. On this basis, as well as from the visual and experimental determinations, the coverage of plated material on the target appeared adequate.

c. Determination of Distribution of Plated Material

A 0.050 in. aluminum plate having a 0.030 in. hole drilled through it was placed between the target and detector and connected to an X-Y micrometer arrangement. Careful plotting of the surface intensity, using this setup, revealed a uniform 4000 cpm intensity coming through the pinhole while scanning the target surface.

C. Mounting of Target and Collector

After the determination of target activity followed the instal-
lation of the target and the collector foil as described in Chapter II,
A (section c.) and the installation of the target-collector assembly
into the glass envelope. The final steps consisted of spot welding
of the three main target-collector elements to the lead-throughs
and sealing off of the tube for an experimental run.

Some precautions were necessary to ensure that the glass
spacer (Figure 2, D) did not become contaminated. After several
experimental runs, a stray current of about 10^{-10} amp appeared
between the collector and target. Cleaning of the spacer with hydro-
fluoric acid remedied the situation. Better screening of the spacer
from the bakeout filaments prevented recurrence of the problem.
Using the electrometer, with the target-collector assembly at
atmospheric pressure, to test for current leakage does not work
with the target installed. The beta particles emitted by the target
cause enough ionization in air to give a current reading of about
10^{-10} amp for a few volts potential difference between the target
and collector.

D. Vacuum System Startup

Startup of the vacuum system forepumps followed sealoff of

the Stage III test tube end and installation of a "break seal" in the

argon supply line. A "Tesla Coil leak check" of the vacuum system

followed when the forepump pressure reached 10^{-3} torr. If no

leaks appeared, liquid nitrogen was added to the foreline cold trap

dewars. Liquid nitrogen filling of the high vacuum dewars and

startup of the diffusion pumps followed several hours of cold trapped

rough pumping to eliminate moisture introduced at sealoff. Startup

of the cooling system and of the diffusion pumps followed, as de-

scribed in Chapter II, B. Detaching of the wiring harness, magnet,

and electrometer from the tube and the emplacement of the main

oven took place when the system pressure reached 10^{-6} torr.

E. Bakeout Sequence

Removal of the high vacuum trap dewars and installation of the

trap ovens occurred when the main oven temperature reached 150°C.

Gradual heating to bakeout temperatures of 400° C for the main oven

and 350° C for the trap ovens, over a three to four hour period,

prevented severe temperature gradients in the heated regions of the

system. A bakeout period of 15 hours, upon achieving bakeout

temperatures, proved sufficient to reduce the system pressure to

10^{-9} torr within 24 hours after completion of bakeout.

Initially, the system was left unattended during the bakeout

period. However, several near disasters provided convincing proof

of the need for constant monitoring during bakeout.

Shutdown of the bakeout cycle consisted of switching off the trap ovens, letting them cool to 100° C, removing the trap ovens, letting the high vacuum cold traps cool to about 50° C (before submerging them in liquid nitrogen), and, finally, switching off the main oven heaters. This procedure took about two hours. The main oven fan continued to run until the oven cooled to room temperature. Since considerable heat transfer from the main oven to the traps occurred during the cooling period, it was necessary to re-fill the cold trap dewars after four hours. Thereafter, until completion of the data run, filling of the cold traps took place every eight hours at the rate of one liter of liquid nitrogen for each four liter high-vacuum trap dewar.

F. Preparation for Experimental Run

a. Wiring Harness Connection

Removal of the main oven, installation of the focussing magnet, and connection of the wiring harness and electrometer to the experimental tube, as shown in Figures 7, 8, and 9, occurred when the main oven reached room temperature.
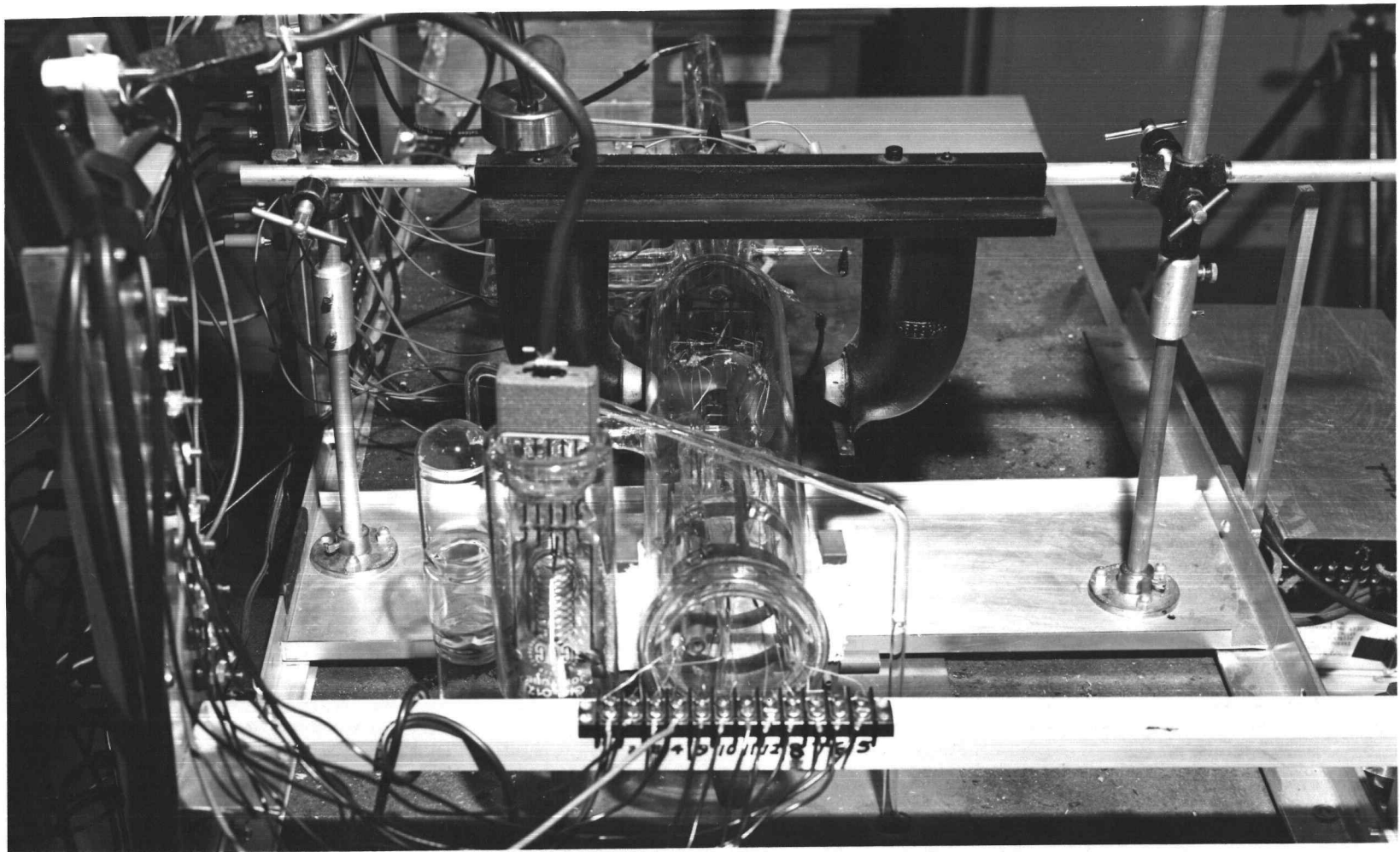
Figure 8.   Stage I electrode connections.
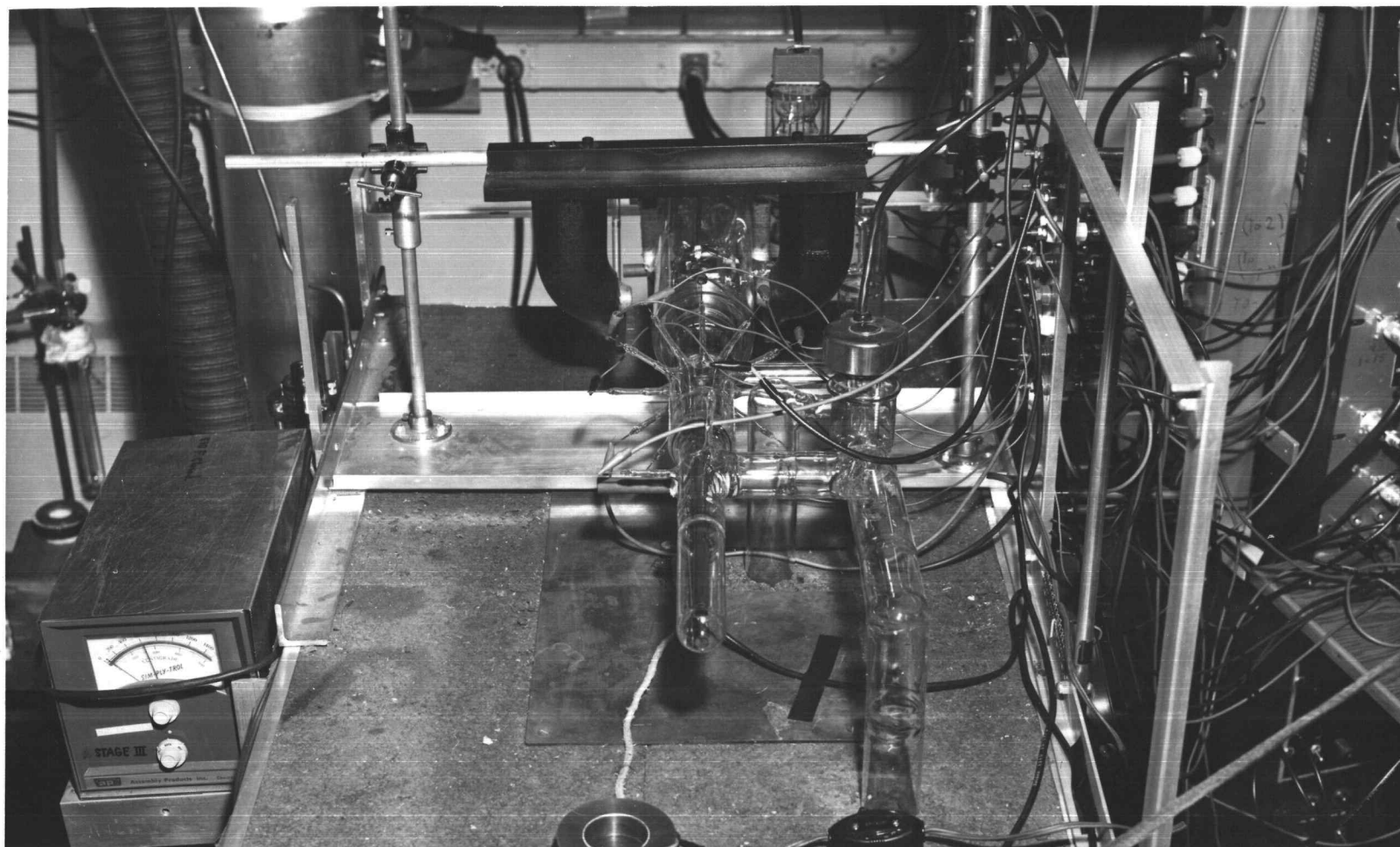
Figure 9. Stage II and Stage III electrode connections.

b. Outgassing and Purging of Argon Supply Line

Startup of the argon supply line forepump, filling of the supply line cold trap when the pressure dropped to 10^{-3} torr, and outgassing and purging of the supply line up to the break seal in front of the high vacuum Granville-Phillips valve preceded outgassing of the experimental tube filaments and introduction of argon into the tube.

Outgassing of the argon supply line, with a heat gun, prior to introducing argon into the line, eliminated the bulk of active gases from the tube walls.

Repeated introduction of argon into the line, at a gauge pressure of 15 psi, and pumping out by the forepump served to reduce the partial pressure of absorbable gases to negligible proportions. Indeed, the limiting factor is seen to be the impurities present in the commercial grade Mattheson argon used for the experiment. Each time the line is purged and refilled, the partial pressure of the original active gases in the line drops another six orders of magnitude. The line was purged ten times before each experimental run and maintained under pressure until completion of the run.

c. Outgassing of the Filaments and Target

The outgassing procedure began with the adjustment of the

magnet to maximize the ion chamber electron current. First, this
was done for a low value of collector current. Then the filament
voltage was increased to give an electron current of about 0.2 ma.
Maintenance of this current level until the Stage III pressure re-
turned to 10^{-9} torr completed the Stage I filament outgassing.

Operation of the target outgassing filaments at 4 amp filament
current for about 15 min degassed the bakeout chamber and fila-
ments. This level of operation was sufficient to yield a good supply
of electrons but low enough to prevent undue evaporation of tungsten.

Introduction of the target, biased at 150 volts with respect to
the filaments, at this point, completed the outgassing procedure.
A series of two to three minute outgassing intervals, totaling about
15 min, seemed to adequately rid the surface of occluded gases.
The pulsed outgassing operation prevented damage to the target sup-
ports from overheating and permitted a gradual pressure decrease,
from one interval to the next, as the de-adsorbed gases were re-
moved.

G. Experimental Run and Shutdown of the System

a. Experimental Run

Cracking of the break seal, which preceded the Granville-
Phillips valve, introduced gas into the system. Adjustment of the

valve with a torque wrench to give a Stage I pressure of about 5 X 10^{-5} torr completed the preparations for the experimental run.

Warm-up and zeroing of the Kiethley electrometer, as well as warm-up of the electrode power supplies, was done while the pressure achieved equilibrium.

Adjusting the power to the ion chamber filament and a final fine adjustment of the tube electrode voltages focussed the ion beam on the target. An ion current of about 10^{-9} amp occurred for sharpest focus. However, somewhat more reproducible results were obtained when the beam was slightly de-focussed. This is probably because the beam covered the target more uniformly instead of focussing on the leading edge of the target which was, in most of the runs, inclined at 30 degrees to the beam. For this reason, the usual bombarding current was 5 X 10^{-10} amp. The typical bombardment time was about 20 min.

At a partial pressure of 10^{-9} torr, the active gases in the system take about an hour to build up to a monolayer on the target. A second degassing of the target was carried out in those runs that took longer than 30 min after completion of the initial outgassing. Shutting off the Granville-Phillips valve and evacuating the argon supply line returned Stage III to 10^{-9} torr for repetition of the outgassing procedure.

b. Shutdown of the System

Switching off the ion chamber filament, power supplies, and diffusion pump heaters brought the bombardment to an end. Removal of the high vacuum cold trap dewars occurred when the diffusion pumps reached room temperature. Removal of the forepump dewars followed when the high vacuum cold traps warmed up to room temperature. As soon as the forepump traps reached room temperature, the forepumps were shut off and the system was opened to atmosphere.

c. Analysis of the Collector

The final steps in each run were to crack open the test tube end of the target chamber, remove the target-collector assembly, slip out the collector foil, and insert a new foil for repetition of the just completed sequence in the next bombardment.

Final treatment of the collector foil included coloring the back side of the collector with felt tipped markers to distinguish between the top and bottom halves, scribing lines 1/8 in. apart on the back side (starting from the entrance slit edges), and scribing numbers on the strips in the same order. Cutting of the collector along the scribe marks and placing the individual strips under the G-M counter setup described in Chapter II, D (section d), for one hour count times, yielded the angular distribution of sputtered material.

IV. EXPERIMENTAL RESULTS AND INTERPRETATION
OF DATA

A. General Nature of Experimental Results

Analysis of the collector foils revealed a series of maxima

and minima over almost the entire 180° through which the ejected

atoms were collected.

Changing the angle of incidence of the bombarding ions merely

shifted the entire pattern by the amount of change in the angle of

incidence. For a given angle of incidence, it appeared that there

was no simple relationship between bombarding energy and the

heights of the observed peaks in the curves of yield versus angle,

except that they all increased with energy. The distribution of

ejected atoms for 100 ev incident ions, as shown in Figure 10, is

typical of the observed ejection patterns. Figure 11, B shows, in

addition to some other information, the relative positions of the

target and collector. It also makes clear the angular designation

used in Figure 10.

B. Interpretation of the Angular Distribution Pattern

a. General Approach

Since the experimental data in no way resembled previously

published results for sputtering of polycrystalline material, it
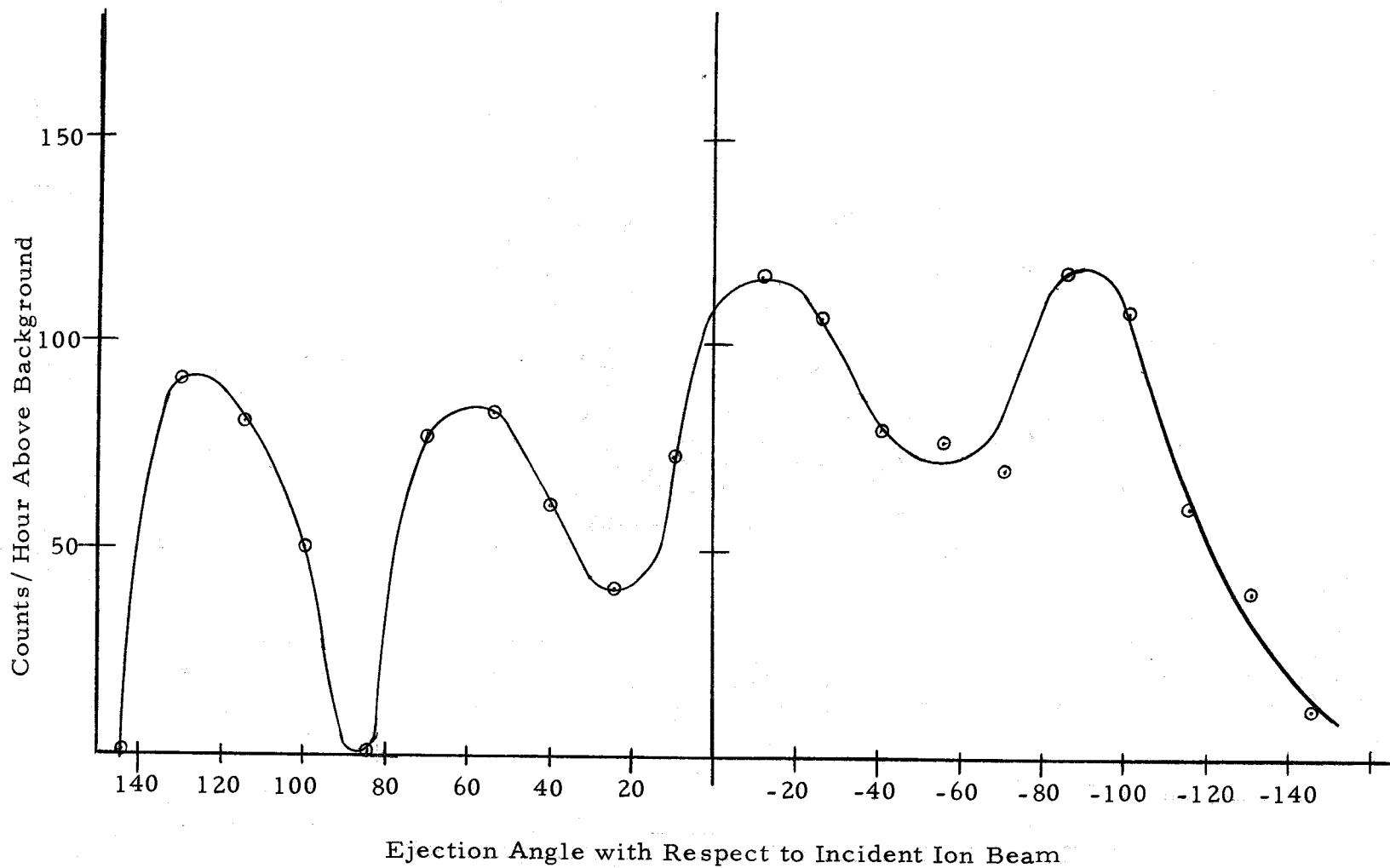
Figure 10. Angular distribution of ejected nickel atoms for 100 ev bombardment.
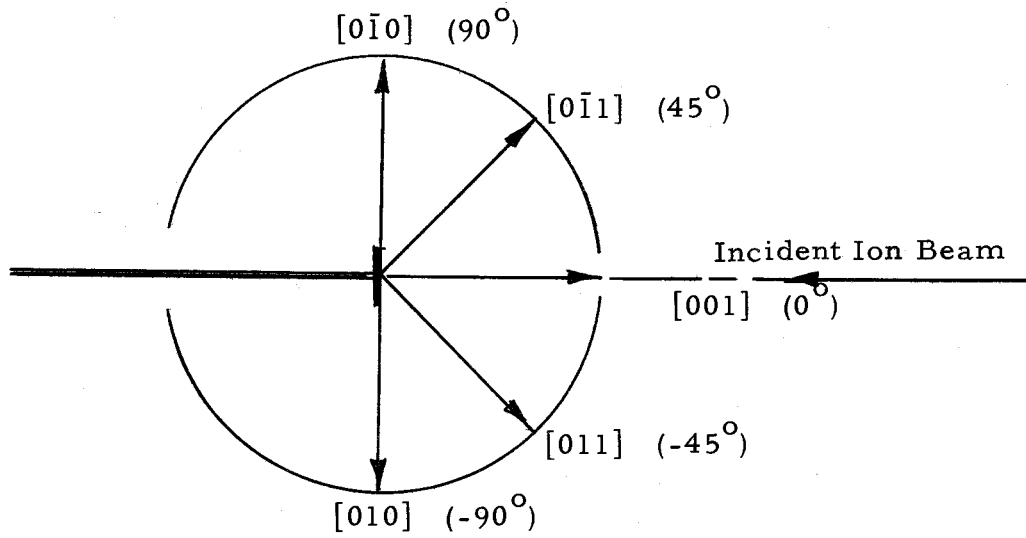
Figure 11-A
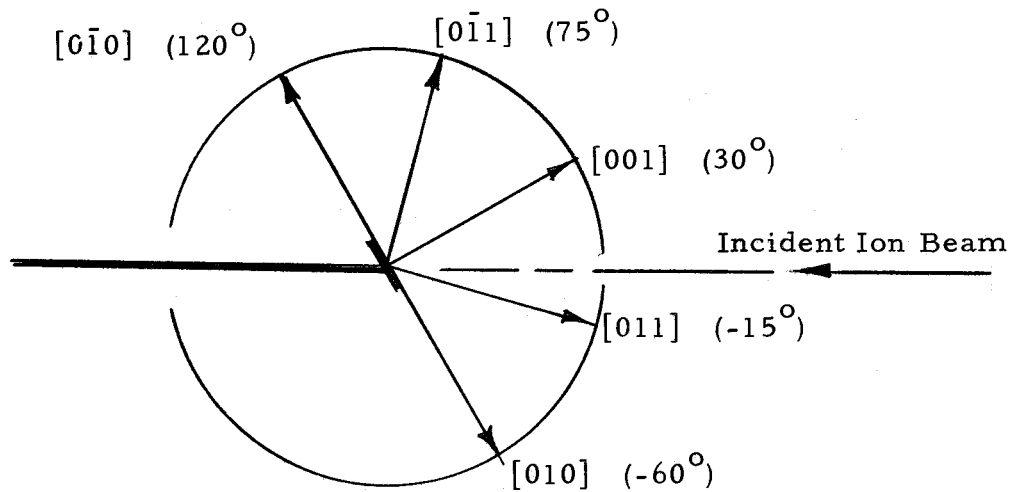
Figure 11-B

Figure 11. Projection of principal crystallographic directions of the target onto the collector.

appeared that some sort of "ordering" of the target had taken place.

A coherent interpretation of the data became possible on the basis

of three assumptions: (1) that the target recrystallized after

heating so that the (001) crystal plane coincided with the plane of

the target and that the ⟨100⟩ direction became aligned with the

target and collector axis (The dimensions of the target were 1/8 in.

by 3/8 in., as described in Chapter III, A. The 3/8 in. dimension

was parallel to the collector axis and to the beam entrance slit into

the collector), (2) that ejection of atoms occurred mainly in the

principal crystallographic directions, and (3) that first order

spectral reflection accounts for the peaks observed behind the target.

b. Target Recrystallization

Reference to Elements of Physical Metallurgy, by Guy (1960),

revealed that cold-rolled copper sheet, when heated to its re-

crystallization temperature, recrystallizes in a definite structure.

In the resultant re-orientation, the [100] direction becomes oriented

parallel to the direction of original cold rolling, and the (001) plane

coincides with the plane of the specimen. Table II compares some

of the properties of copper and nickel that might be expected to have

a bearing on the recrystallization process in the two materials.

Table II. Recrystallization Parameter Comparison

Parameter	Copper	Nickel
Crystal Structure	fcc	fcc
Nearest Neighbor Distance	2.556 A	2.491 A
Recrystallization Temperature	204° C	590° C

As already indicated, the nickel substrate for the target was cold-rolled nickel foil. Heating the nickel target to a barely discernable redness, by electron bombardment, during outgassing, definitely brought the target temperature above that required for the recrystallization of nickel. In view of the structural similarity of copper and nickel, the first assumption, in unraveling the data, was that the target recrystallized in the same form as described for copper. X-ray diffraction analysis of the target, upon completion of all test runs, showed that this assumption was correct.

Analysis of a second-order x-ray diffraction pattern of the nickel target revealed that it consisted of very small microcrystals, approximately 80 percent of which were aligned with a (100) plane coinciding with the target surface and with a $\langle 100 \rangle$ direction parallel to the longest dimension of the target. The longest dimension of the target, in turn, was parallel to the collector axis and to the ion beam entrance slit in the front of the collector. The results of the x-ray powder pattern, shown in Figure 12, indicated the relative intensities

Average polycrystal diameter: 600Å--800Å
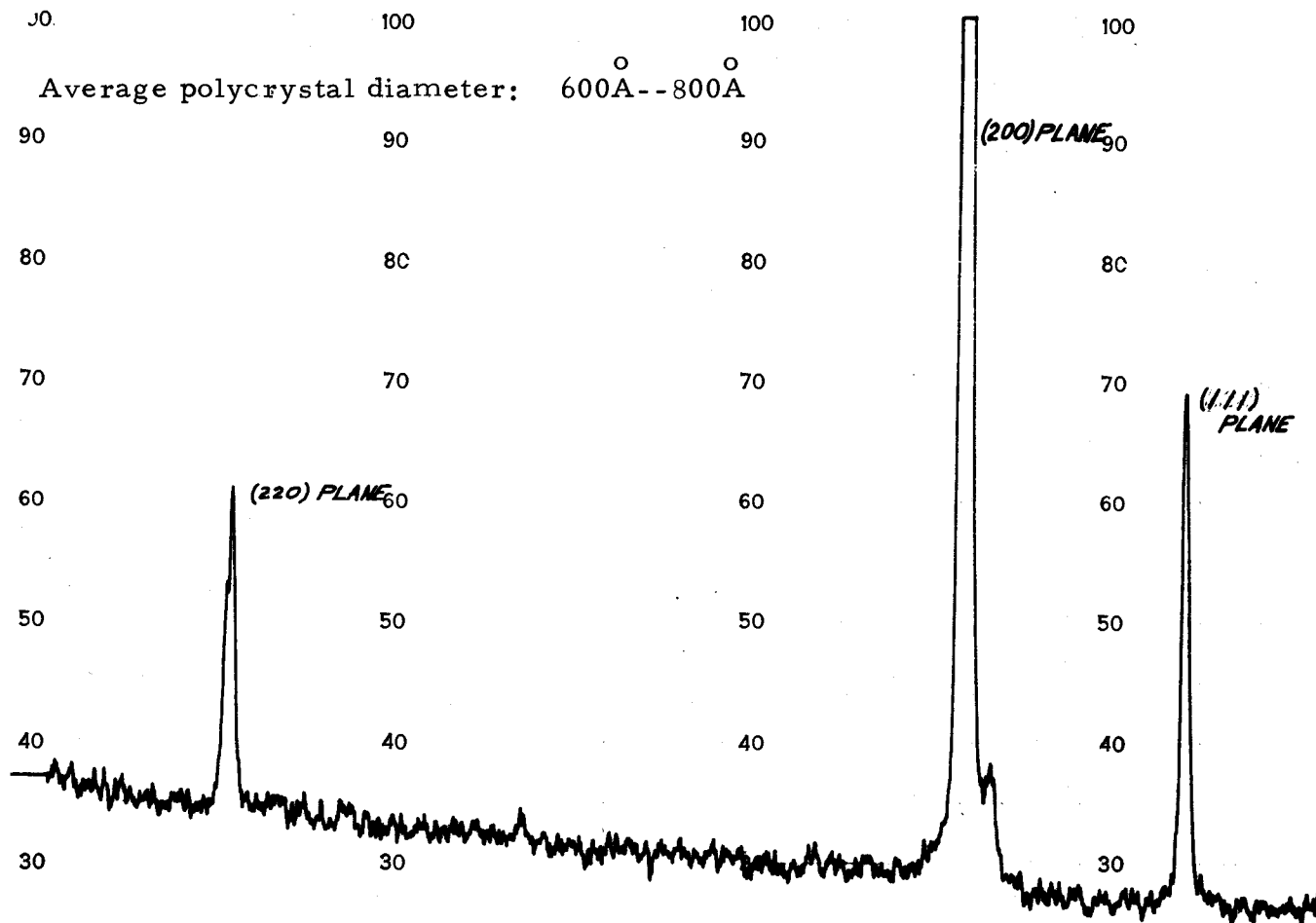
Figure 12.   X-ray diffraction pattern of the target.

of 2.7, 20, and 1.7 for diffraction from (111), (200), and (220)

planes, respectively. The respective values for a perfectly random

pattern are 1.00, 0.42, and 0.21.

c. Proposed Model for Atomic Ejection

Since the single crystal sputtering data (Wehner, 1956; Koedam,

1961), to cite only two examples, indicates that preferential sputter-

ing occurs in the $\langle 110 \rangle$ and $\langle 100 \rangle$ directions for nickel, the second

assumption made was that ejection of atoms occurs primarily from

the ends of those rows of atoms in a crystal which terminate on the

surface. Figure 11 indicates the angles at which maxima might be

expected for such a model, for normal ion incidence and for 30°

incidence. The crystal structure assumed is that proposed in the

previous section. The direction normal to the target is the [001]

direction; that which is parallel to the target and coming out, per-

pendicular to the plane of the paper, is the [100] direction. More

exactly, Figure 11 shows the extension of those principal directions

which lie in the (100) plane. The positions at which these extensions

intersect the collector should, then, coincide with maxima of the

observed distribution. Recalling that the collector was cut into

strips to yield the angular distribution of sputtered atoms, ejection

from azimuthal directions not normal to the collector (i.e., not in

the (100) plane) should appear as though it originated from the

projection of the non-normal directions onto the (100) plane. More specifically:

$[\bar{1}11]$ and $[111]$ project onto the $[011]$ direction,

$[1\bar{1}1]$ and $[\bar{1}\bar{1}1]$ project onto the $[0\bar{1}1]$ direction,

$[110]$ and $[\bar{1}10]$ project onto the $[010]$ direction, and

$[\bar{1}\bar{1}0]$ and $[1\bar{1}0]$ project onto the $[0\bar{1}0]$ direction.

The other directions which, if extended, come out of the target plane, are the $[001]$, $[100]$, and $[\bar{1}00]$ directions. Since the latter two have no projection onto the (100) plane, one should thus observe maxima on the collector corresponding only to the $[001]$, $[011]$, $[0\bar{1}1]$, $[0\bar{1}0]$, and $[010]$ directions. This is shown in Figure 11, for normal and 30° ion incidence. Projections of the target boundaries, parallel to the principal directions, intersected arcs of about 10° on the collector surface. Thus, the location of the maxima should occur within plus and minus five degrees of the positions indicated.

Examination of the data curves showed good agreement with the proposed model. The data handling technique appears, schematically, in Figure 13. Here, the maxima of Figure 10 are tentatively divided into symmetrical peaks. Comparison of the location of these maxima with predicted positions provides a test for the validity of the proposed model. For the most part, maxima occurred where predicted. Occasionally, predicted peaks did not appear. In one or
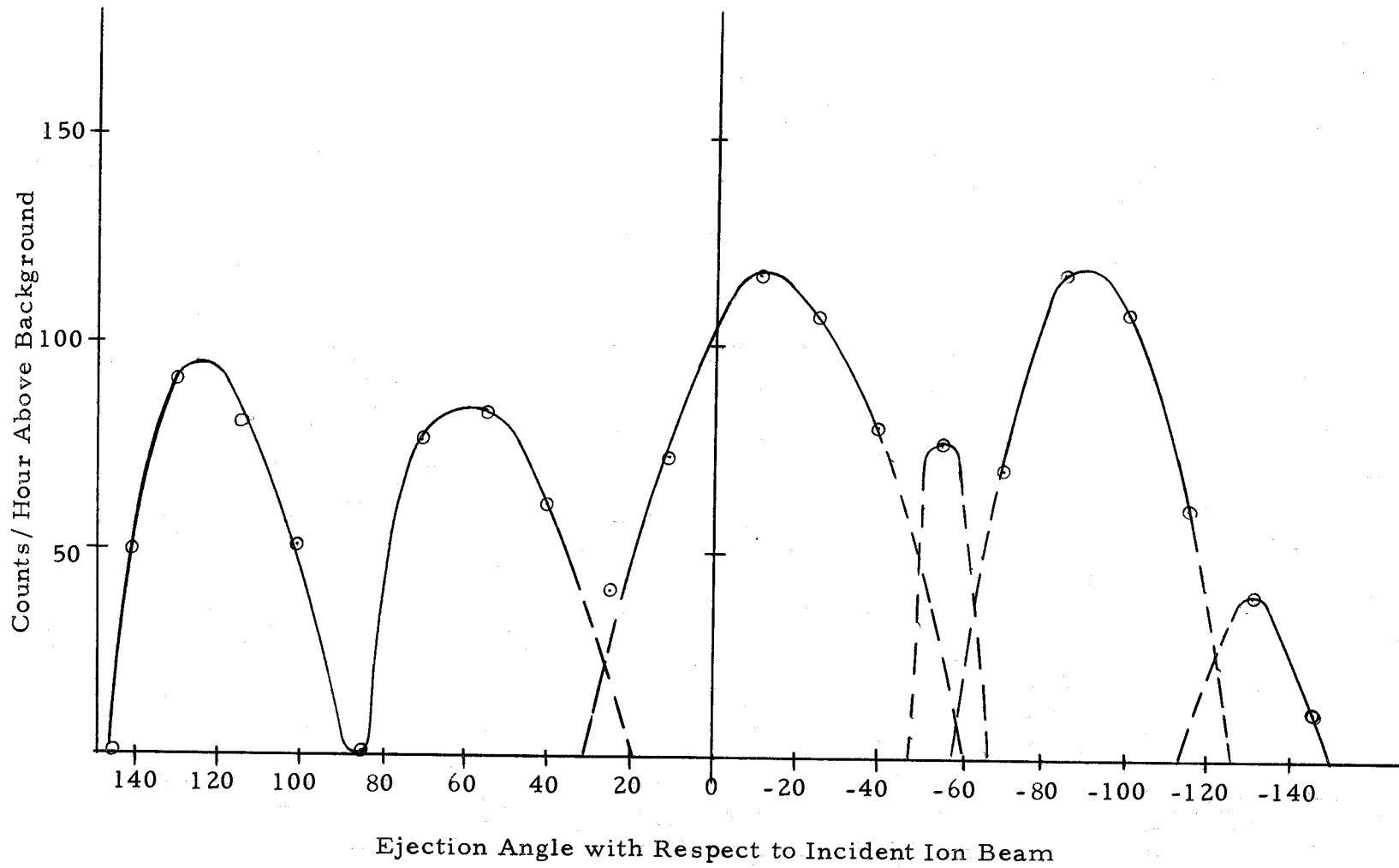
Figure 13. Resolution of individual maxima of ejected nickel atoms for 100 ev bombardment.

two instances, an unexpected maximum occurred just outside the predicted location. However, correction for the reflection peaks, which occurred behind the target, gave essentially complete agreement with the proposed model. The reflected components combined with the primary peaks to give maxima where predicted. Also, correcting for reflection, in all instances, restored "missing" maxima.

C. Correction for Reflection

Because the reflection data are of interest in their own right, apart from being part of the sputtering yield data, a more complete discussion of the observed reflection maxima appears in a later section. It suffices here to note that the assumption of first order specular reflection seems to give an adequate explanation of the observed maxima behind the target (as far as analyzing the sputtering data is concerned). If the target were perfectly centered, the bulk of the reflected material would return to it. Any observed reflections would be due to small amounts of reflected material which barely missed the target edges. The target, perhaps fortuitously, was not perfectly centered in the direction of the beam. Since a complicated pattern was unexpected, the lateral centering of the target was "visual." Also, because of the long cantilever support required for moving the target in and out of the collector

chamber, a certain amount of flexibility was inevitable in the

transverse direction as well. The inside diameter of the collector

foil was 15/16 in. Careful measurement showed that the target axis

was 1/16 in. behind the axis of the collector. A scale drawing,

Figure 14, shows the relative positions of the target and collector

during bombardment and enables one to determine where the reflec-

tion maxima ought to occur, assuming specular reflection.

The primary maxima are indicated in Figure 14 as occurring

at 124°, 80°, 33°, -17°, and -64°. This is not significantly differ-

ent from the locations predicted by a perfectly centered geometry.

Consideration of the reflection from the 80° primary maximum

shows that atoms ejected at A deposit at position 1 on the collector.

Specular reflection requires that some of this material transfers to

position 1'. Similarly, material originating at the target axis and

edge B, of the target, deposits at positions 0 and 2 respectively,

from which some reflects to positions 0' and 2', respectively. If 0

is at the center of the 80° maximum, then a reflection maximum

should occur at 0'. Similar analysis, for the primary maxima at

33°, -17°, -64°, and 124° predicts reflection peaks in the vicinities

of -140°, 160°, 116°, and -44°, respectively.

It appears that the 33° and -17° maxima should only reflect

material, which originated from the lower half of the target, to the

corresponding reflection peaks on the opposite side of the collector.
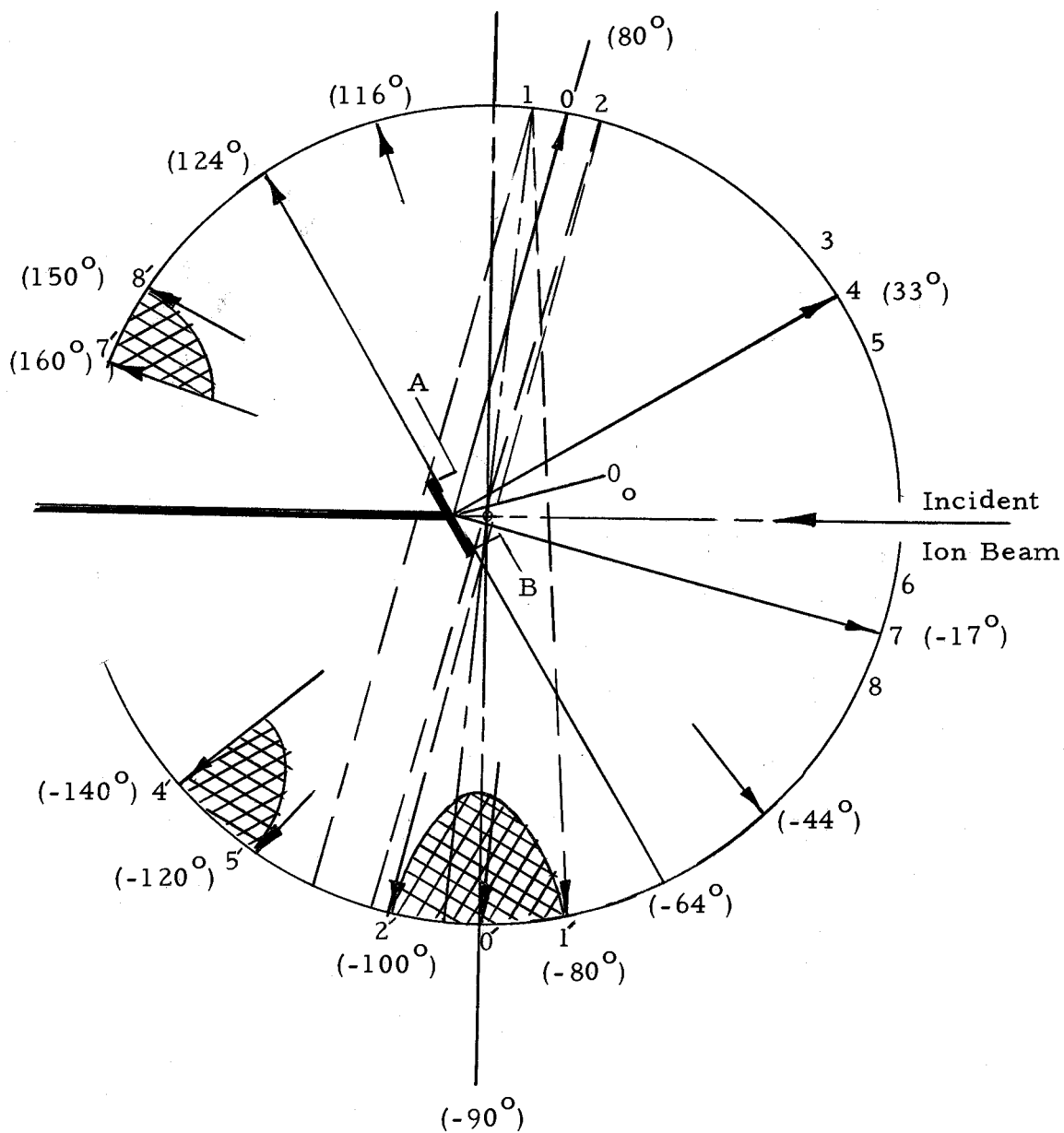
Figure 14. Determination of reflection peak location assuming specular reflection.

Material originating from the top half of the target, when reflected from the collector, should hit the target and not return to the collector to contribute to a reflection peak. However, several features of the yield data indicate that the return to the target of a large fraction of the reflected material did not occur. The reflection maxima corresponding to the 33° maxima were much more symmetrical than one would expect if the target had intercepted a large fraction of the reflected atoms; their shape and half-widths were similar to those for the 80° primary maxima. Reflection ratio curves for the 33° and 80° primary maxima, Figure 19 in Part F of this Chapter, exhibit similar behavior. This also indicates that little, if any, material reflected from the 33° maximum encountered the target on reflection. In addition, the angular maxima tended to occur at slightly smaller angles than predicted. The explanation appears to be that most of the ion beam focussed onto the bottom half of the target and that, in fact, the target intercepted very little reflected material.

Reflection from the collector at 124° and -64° to -44° and 116°, respectively, either did not occur, or, as seems more likely, was sufficiently small to be buried between the adjacent maxima. The other reflection peaks appeared where predicted.

Superimposing of the reflection maxima onto their corresponding primary peaks yielded the family of curves shown in

Figure 15. Normally, the reflected distribution should be broadened over that of the primary. This did not occur for either the 33° or 80° maxima. A more detailed study of the reflection data, in Part F, shows that most of the reflected atoms probably came from the center region of the primary maxima and indeed were quite well focussed. Thus, not much broadening occurred, and, to a good approximation, the total relative yield is the sum of the primary and reflected maxima. The maximum value of each peak thus represents the relative yield at the given angle and bombarding energy.

It is noted that considerable yield appears at angles greater than 120°. This is probably because it was not possible to separate out the reflection peaks originating from the -17° position. Generally, the trend of increasing yield with increasing energy is quite clear, except for the -64° and 124° maxima. There, one expects poor consistency in the data because of tangential ejection, non-grazing incidence of the ion beam, and interference of the target support.

Since the -17° maxima do not include reflected material, and the -64° and -124° maxima are not very consistent, only the 80° and possibly the 33° maxima appear suitable for a direct quantitative analysis of the relative yield versus bombarding energy. However, the possibility of correcting the -17° maxima for reflection exists. Before converting the angular distribution data of Figure 15 into the
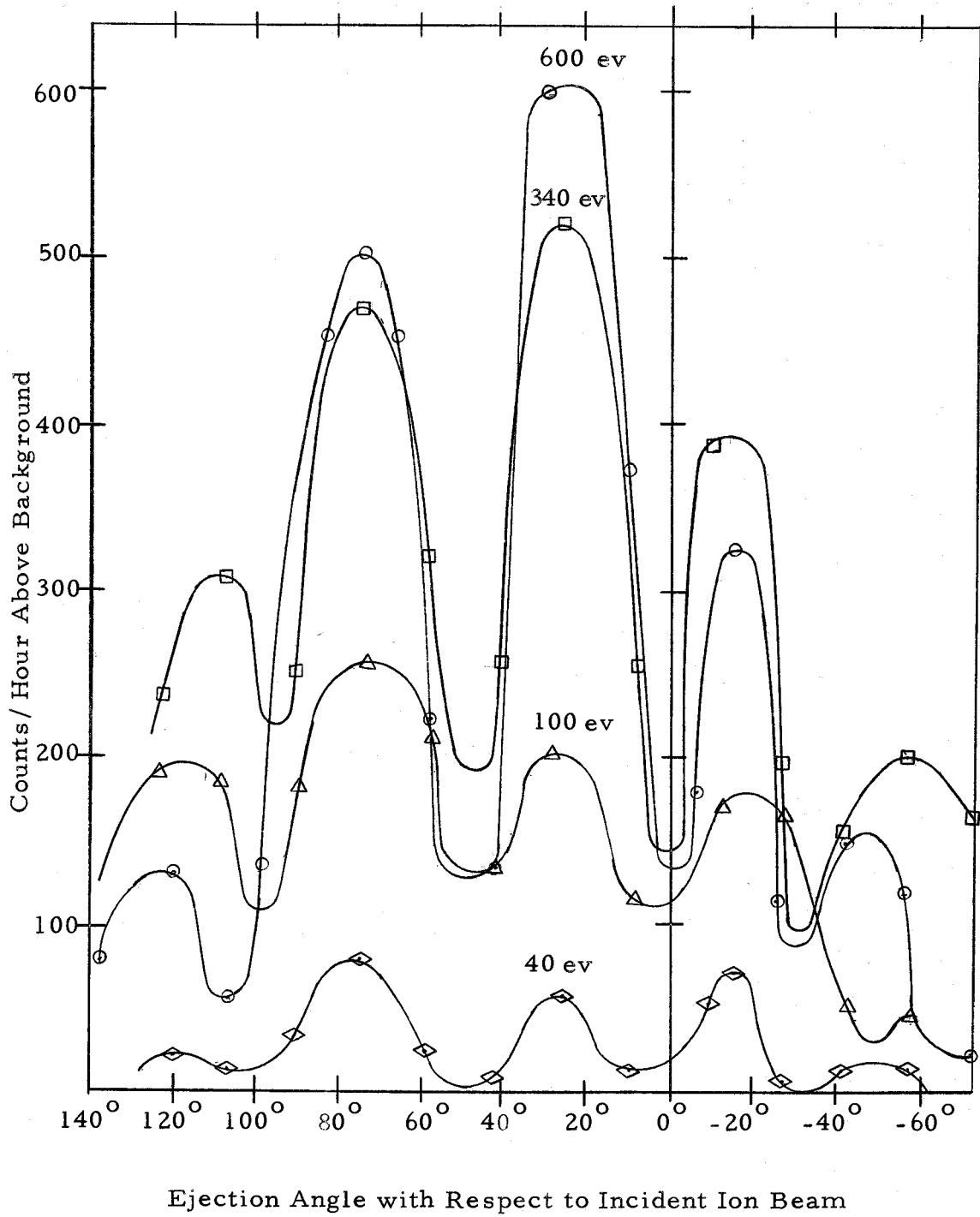
Figure 15. Angular distribution of nickel atoms sputtered from a (100) plane, inclined at 30° to the incident argon ion beam, as a function of bombarding energy.

standard relative yield curves, it is necessary to investigate the

azimuthal distribution of sputtered atoms. This is to define, more

precisely, the meaning and limitations of the resulting relative yield

curves.

D. Azimuthal Distribution of Ejected Atoms

In view of the structured nature of the angular data, it seems

appropriate to inquire as to the expected azimuthal distribution. A

ray diagram analysis, Figure 16, similar to that used for the

angular distribution predictions, suffices. As is noted, Sections

A-A, B-B, and C-C through the collector, predict the positions of

azimuthal deposits for directions tangential, normal, and at 45°,

respectively, to the target.

Wehner, Koedam, and others, as already indicated, report

that preferential sputtering from the (100) plane of nickel occurs in

the $\langle 110 \rangle$ and $\langle 100 \rangle$ directions. There exists no report of sputter-

ing from the $\langle 111 \rangle$ directions of nickel for bombarding ion energies

below 1000 ev. On this basis, the collector should exhibit strong

azimuthal maxima near the edges for directions tangential and nor-

mal to the target, and at the center of the collector for directions

at 45° to the target. These correspond to $\langle 110 \rangle$ ejection directions.

Less pronounced maxima should occur, azimuthally, at the center of

the collector for the $\langle 100 \rangle$ directions pictured in Figure 16.

[ī̄10] [Ī00] [ī10]

(124° and -64° maxima)

Tangential

A
A

[1ī0] [100] [110]

Sec. A-A

[101] [001] [ī01]

(33° maxima)

Normal

B
B

Sec. B-B

[1ī1] [0ī1] [ī11]

(-17° and 80° maxima)

45°

C
C

Sec. C-C
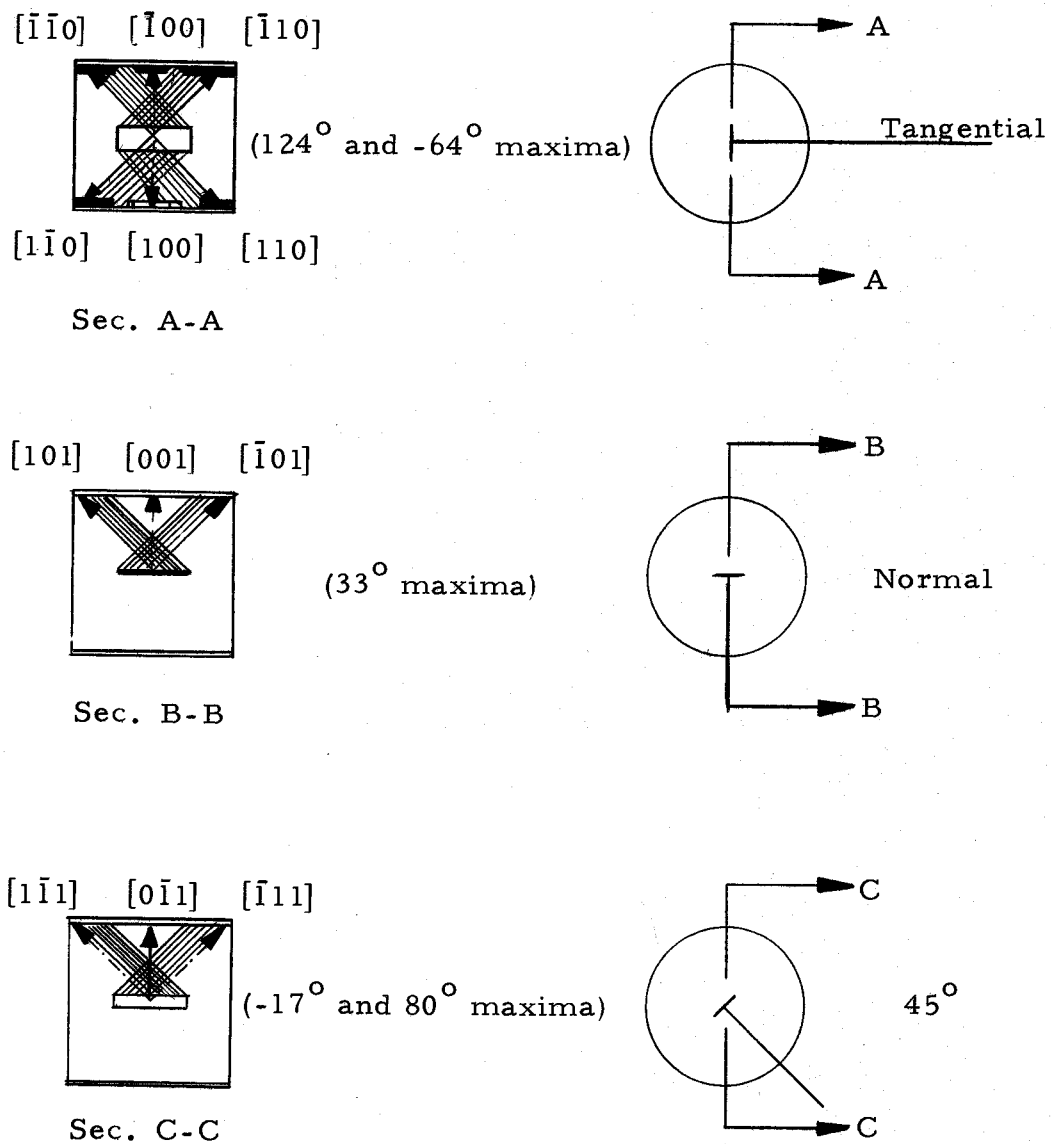
Figure 16. Derived azimuthal distribution.

Perhaps the most interesting prediction is that for the maxima seen at 45°, with respect to the target normal, in the angular distribution. If, indeed, no sputtering occurs in the $\langle 111 \rangle$ directions, activity observed at 80° and -17° occurs, azimuthally, at the center of the collector and is due entirely to sputtering from the $[0\bar{1}1]$ and $[011]$ directions, respectively.

On the basis of the specular reflection model, which accounts for the anomalous peaks found behind the target, the reflected peaks should come only from the azimuthal center of the collector. Ejected atoms leaving at an azimuthal angle of 45° with respect to the target, if reflected, leave the collector chamber and deposit on the tube walls. Only atoms which hit the collector at approximately normal azimuthal incidence can be collected on reflection. Thus, the reflection maxima at 160° and -90° must be due entirely to ejection from the $\langle 110 \rangle$ directions of the -17° and 80° maxima, respectively. That at 140° must come from the $[001]$ direction of the 33° maximum.

A radioautograph of four collector foils, re-assembled from their component strips, after completion of angular distribution measurements, proved inconclusive. A four day exposure of x-ray film, placed in contact with the collectors, produced the radioautograph. Since the collector was re-assembled from its components, good contact with the collector was not possible. A

continuous distribution of points did not appear. Rather, the activity

on the film consisted of a collection of small local hot spots about

0.05 cm in diameter. In general, the radioautograph pattern

seemed in qualitative agreement with the predicted behavior.

E. Relative Yield Curves for 33°, 80°, and -17°

a. Introduction of Relative Yield Data

Figure 17 shows the intensities of the $80°$, $33°$, and $-17°$

peaks of Figure 15 as a function of incident ion energy. A similar

yield curve, shifted to the left so that its threshold energy coincides

with that of this study, from an experiment by Laegreid and Wehner

(1961), indicates typical results obtained by other investigators for

the sputtering of polycrystalline nickel by argon ions, in the 50 ev to

600 ev energy range.

Correction of the $-17°$ data from Figure 15 for reflection and

normalizing the half-widths of the $-17°$ maxima to those of the $80°$

maxima results in the $-17°$ relative yield curve shown.

b. Discussion of Relative Yield Curves

It is noted that all the curves shown in Figure 17 have an

identical slope near threshold. The experimental data indicate a

threshold energy for sputtering of about 18 ev for the $80°$ yields and
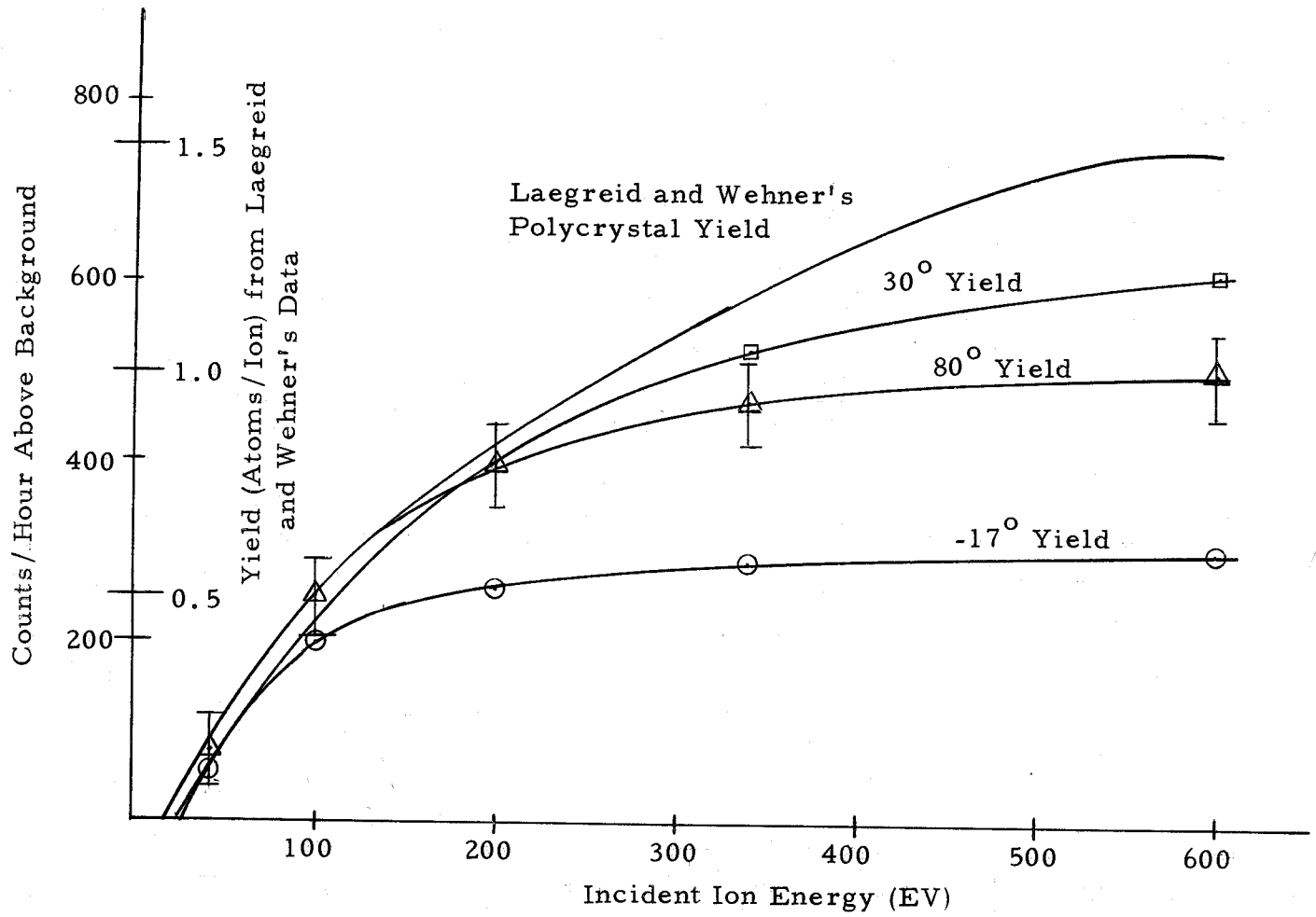
Figure 17. Relative yield curves.

about 25 ev for the -17° yields. The lowest data point in the extrapolation to threshold was for a 25 ev bombardment, as compared to more than 50 ev for Laegreid and Wehner's data. Their curve intersected the energy axis at 50 ev, though Wehner (1961), more recently, published a threshold value of 21 ev for nickel bombarded by argon ions. Too high a threshold energy indicates surface contamination (Wehner, 1955), or insensitive yield measurement techniques. This results in too low a yield, particularly at the lower bombarding energies. Thus, shifting the polycrystalline yield curve so that its threshold occurs at 18 ev, as measured in the present experiment, probably represents the typical nickel-argon yield curve more realistically than does Laegreid and Wehner's published curve.

The shape of Laegreid and Wehner's curve is typical for sputtering either from a polycrystal or from a (100) plane of a single crystal fcc material. In either case, the curve levels off and saturates in the vicinity of about 2000 ev, rather than at 300 ev or 400 ev as indicated for the 80° and -17° curves. The 33° curve, which results from sputtering from a mixture of $\langle 110 \rangle$ and $\langle 100 \rangle$ directions, lies between the yield curves from the $\langle 110 \rangle$ directions at -17° and 80° and the polycrystalline curve. In either the sputtering of polycrystals or oriented single-crystals, sputtering occurs from a combination of $\langle 110 \rangle$ and $\langle 100 \rangle$ directions. This assumes,

as reported, that no sputtering takes place from the $\langle 111 \rangle$ directions. For the -17° and 80° maxima, as indicated, the yield measured was entirely from the $\langle 110 \rangle$ directions.

A rapid saturation of yield as a function of energy, similar to that for the 80° and -17° data, occurred in a Field Ion Microscope study of sputtering by Strayer, Cooper, and Swanson (1965). They used Cs^{+} ions for the incident particles and counted the number of atoms removed from the principal planes of a (110) oriented tungsten field emitter. An analysis of their data shows that a $\langle 111 \rangle$ principal axis was perpendicular, or nearly so, to each of the planes which yielded a sizable fraction of all atoms sputtered.

Experimental studies of ejection patterns from single crystals have shown that sputtering occurs first from directions of closest packing. Then, upon sufficient increase of bombarding ion energy, it occurs also from the next-closest-packed directions--the $\langle 100 \rangle$ directions for fcc materials. The respective directions of closest packing for fcc and bcc materials are the $\langle 110 \rangle$ and $\langle 111 \rangle$ directions. Anderson (1962) noted that for the case of bombardment of a (110) surface of a fcc crystal, which is of most interest here, the ejection from the $\langle 100 \rangle$ directions was so weak compared to that from the $\langle 110 \rangle$ directions that it was seldom seen at energies less than 800 ev. It is noted that the superposition of two separate yield curves having different threshold energies would yield the observed

polycrystalline curve. Both the present experimental study and the data of Strayer, Cooper, and Swanson seems to indicate that this actually is the case. Anderson's observation of delayed emission from $\langle 100 \rangle$ directions adds additional proof.

Another feature of sputtering shown by the curves of Figure 17 is that, at low energies, the sputtering yield is nearly independent of the orientations of the closest-packed ejection directions. However, a comparison of the -17° curve, derived from the raw data in the next section, and 80° curves shows that the "saturation yield" is a sensitive function of orientation.

In summary, a comparison of polycrystalline sputtering yields with $\langle 110 \rangle$ directional yield curves, shows that (1) the single-direction sputtering yields saturate much sooner than those for poly-crystalline material, or for sputtering from an entire principle plane (from here on referred to as "whole plane" sputtering), (2) at low energies, the yield is nearly independent of the orientation of the close-packed ejection directions, (3) as energy increases, the "saturation yield" becomes a sensitive function of the orientation of the closest-packed ejection directions, (4) the extrapolated sputter-ing thresholds appearing in the literature appear meaningful only when applied to sputtering from the directions of closest packing, and (5) the sputtering yield curves in the literature consist of the superposition of saturated yield curves for sputtering from the

directions of closest packing and the next-closest-packed directional

yield curves, which have a higher threshold energy.

c. Determination of -17° Relative Yield Curve

Figure 18 indicates, schematically, the normalization process

for the -17° data. The middle curve is a plot of the values of the

-17° maxima of Figure 15. These peaks, unlike the total intensity

peaks at 80° and 33°, include no reflected component. The reflec-

tion conditions for -17° are identical to those for the 80° curve. In

both instances, ejection of sputtered atoms is from a $\langle 110 \rangle$ direction

which is normal to the collector. Thus, the curve of reflected

intensity divided by total intensity for 80° (Figure 19) permits calcu-

lation of the total intensity for the -17° maxima. The top curve of

Figure 18 is the result. However, it is noted that the 340 ev and 600

ev maxima, at -17° are much narrower than those at 33° and 80°.

This means that much less material was sputtered at the -17° loca-

tion than at 80° or 33°. Multiplying the values of the points on the

top curve by 0.5, since the half-widths of the -17° peaks are roughly

50 percent of those of the 80° maxima, yields the bottom curve.

This result is taken to be the "corrected" relative sputtering yield

at -17°.
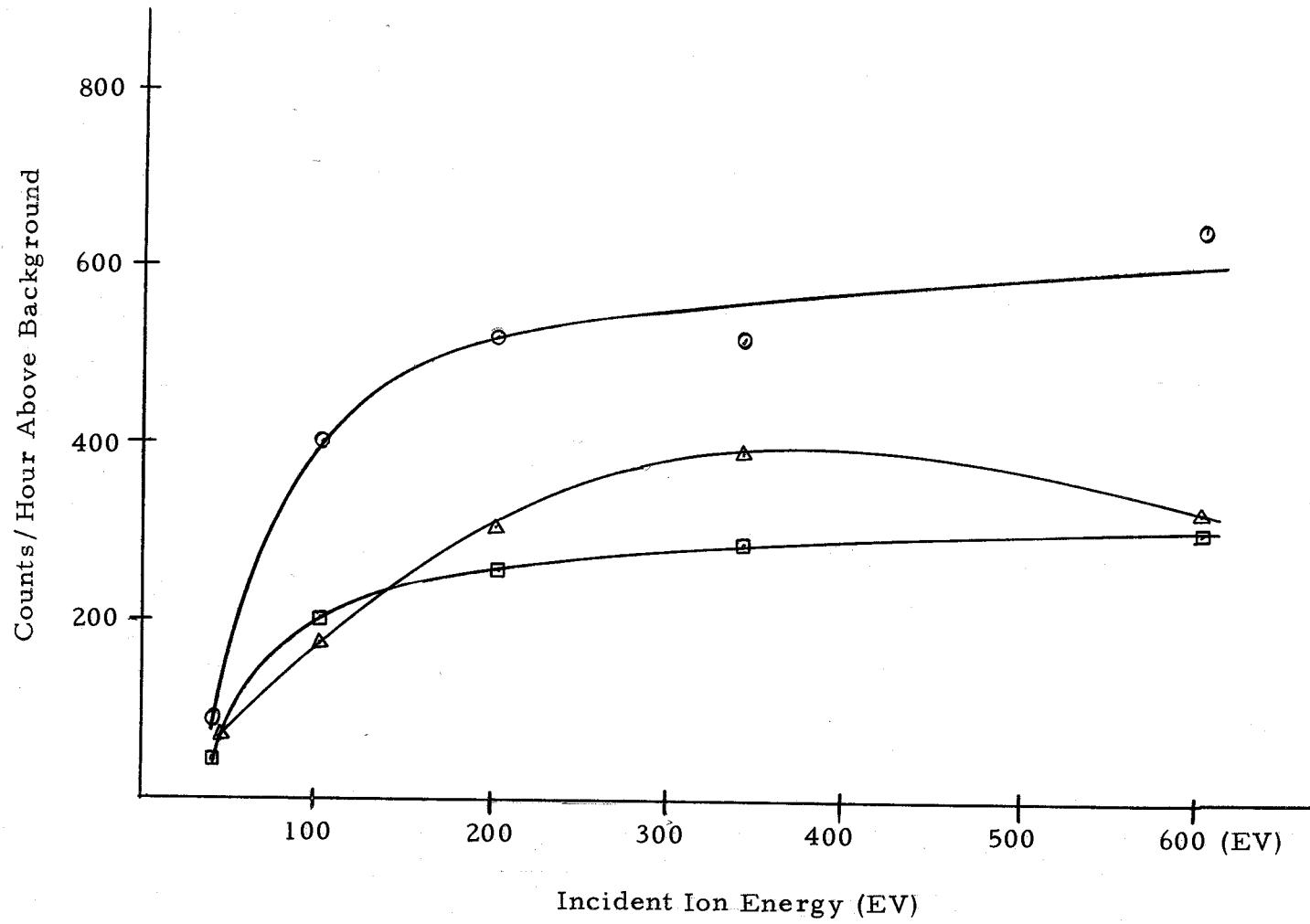
Figure 18. Normalization of -17° data.

F. Survey of Research on Reflection in the Case of
Strong Attractive Forces and Discussion
of Observed Reflection

a. Summary of Current Status of Reflection Research

A literature search revealed that for strong attractive forces,
as is the case when a metal atom impinges onto a metal substrate,
one expects no reflection unless the energy of the incident atoms is of
the order of 100 ev. Furthermore, if it does occur, it "should" be
diffuse, or cosine, rather than specular reflection. These conclu-
sions follow largely from theoretical arguments, though experimental
work does exist in the thermal energy range for Maxwellian energy
distributions of incident particles.

b. Theoretical Conditions for Reflection

Calculations by Cabrera (1959) and Zwanzig (1960) indicate that
reflection is not expected for strong interactions unless the incident
particles have energies that are at least 25 times that of the desorp-
tion energy E_D, which is the binding energy of an adsorbed atom.
Since desorption energies of metal atoms on a metallic substrate are
typically 1 ev to 4 ev (Hirth and Pound, 1963), this requires particle
energies of 25 ev to 100 ev for reflection to occur. The model used
for these theoretical studies was a one-dimensional, semi-infinite
array of connected masses impinged upon by an atom. Cabrera

assumed a harmonic interaction potential cut off at the limit of the

range of surface forces but noted that this may be too "soft" a poten-

tial. He states, however, that even the use of a more realistic inter-

action potential should not decrease the required energy 25 E_D to less

than 10 E_D. Zwanzig performed calculations for several similar

potentials and got essentially the same results. These efforts repre-

sent a classical approach to reflection that should be valid for all but

light gas molecules reflecting from a surface. The quantum-

mechanical version of these calculations is a many-phonon problem.

Hirth and Pound (1963), in a recent review volume, state that the

cosine law of reflection is expected if (1) the incident molecules are

in thermal equilibrium with the surface, i.e., the reflection surface

is in equilibrium with a vapor phase which has a Maxwellian distribu-

tion, (2) the momentum is entirely accommodated so that the hori-

zontal components of momentum reflect randomly, and (3) scattering

occurs from surface irregularities. Unless an experiment consists

of observing reflection of light gases from cleaved crystals, at low

energies, the third case should ensure diffuse reflection. The con-

dition for reflection from surface irregularities is

$$h_I \, \text{Cos} \, \theta \geq \lambda_I$$

Where λ_I is the deBroglie wavelength of the incident atom, θ_I is the

angle of incidence, and h_I is the average height of surface

irregularities. For mechanically polished metal surfaces, the latter is usually of the order of 10^{-5} cm.

c. Typical Experimental Studies

Recent experiments by von Goeler and Lüsher (1961) and von Goeler and Peacock (1963) indicate that the sticking coefficient of silver on molybdenum is unity. Both of these experiments utilized atomic beams of radioactive atoms incident on a target in a high vacuum environment (10^{-9} to 10^{-10} torr). Outgassing of the target surfaces was by electron bombardment.

Koedam (1961), in his studies of sputtering, searched for reflection of both sputtered and evaporated atoms from a glass substrate; he concluded that there was none.

Since all the studies appearing in the literature, of reflection of metal atoms from metal substrates, are done at thermal energies, the appearance of strong specular reflection maxima must relate to some feature of the energy spectrum of sputtered atoms.

d. Energy Distribution of Sputtered Atoms

Stuart and Wehner (1964) measured the energy distribution of atoms sputtered from the principal directions, at various angles to the direction of incident ions, for copper single crystals, for ion energies ranging from 80 ev to 1200 ev. At 80 ev, for a [110]

direction inclined at 60° to the target normal, they reported an "almost" Maxwellian distribution of ejection energies with a peak at about 2 ev and which extended to about 15 ev. At 600 ev, the maximum shifted to about 5 ev and the tail of the distribution terminated at about 60 ev.

The results for nickel should be similar to those for copper except that one would expect the maxima to occur at somewhat lower energies. The cohesive energy for copper is about 80 percent that of nickel. The sputtering yields are typically twice as high for copper as for nickel. Their masses are approximately equal. Thus, more energy should be lost by a nickel atom leaving the surface than by a copper atom. Hence, one would expect the energy distribution to shift to slightly lower energies.

e. Summary of Reflection Data

It was noted that the reflection and primary maxima were of comparable intensity, and, as indicated, there was no evidence of second order spectral reflection.

All efforts to fit a cosine distribution to the reflection data failed. A line source of diffusely ejected atoms from a cylindrical surface yields an angular distribution of

$$I(\theta) = \frac{I_o}{4a^2 \cos\theta}$$

where a is the cylinder radius and θ is the angle of reflection measured from the normal. The location of the line source on the cylinder is taken to be the origin. This angular distribution is completely at variance with the experimental results found in the present investigation.

A somewhat disturbing feature of the reflection data is that the reflection maxima half-widths were not significantly different from those of the primary maxima. One would expect some broadening to occur in the reflected peaks.

Figure 19, a plot of the reflection ratio versus the energy of the argon ions incident on the target shows that a maximum in the reflection ratio occurs at about 100 ev ion energy. The reflection ratio is defined as the ratio of the reflected to the total intensity of sputtered atoms, where the total intensity is the sum of the reflected intensity and that of its parent primary maximum.

As was shown previously, the location of the target slightly behind center, in the collector, permitted all atoms reflected from the 80° primary maximum to hit the opposite side of the collector. This was not true of the reflections from the 33° primary maximum. However, plotting the reflection ratios as a function of energy for the 33° maximum, as well, yields considerable agreement, in form, with the curve for 80°.
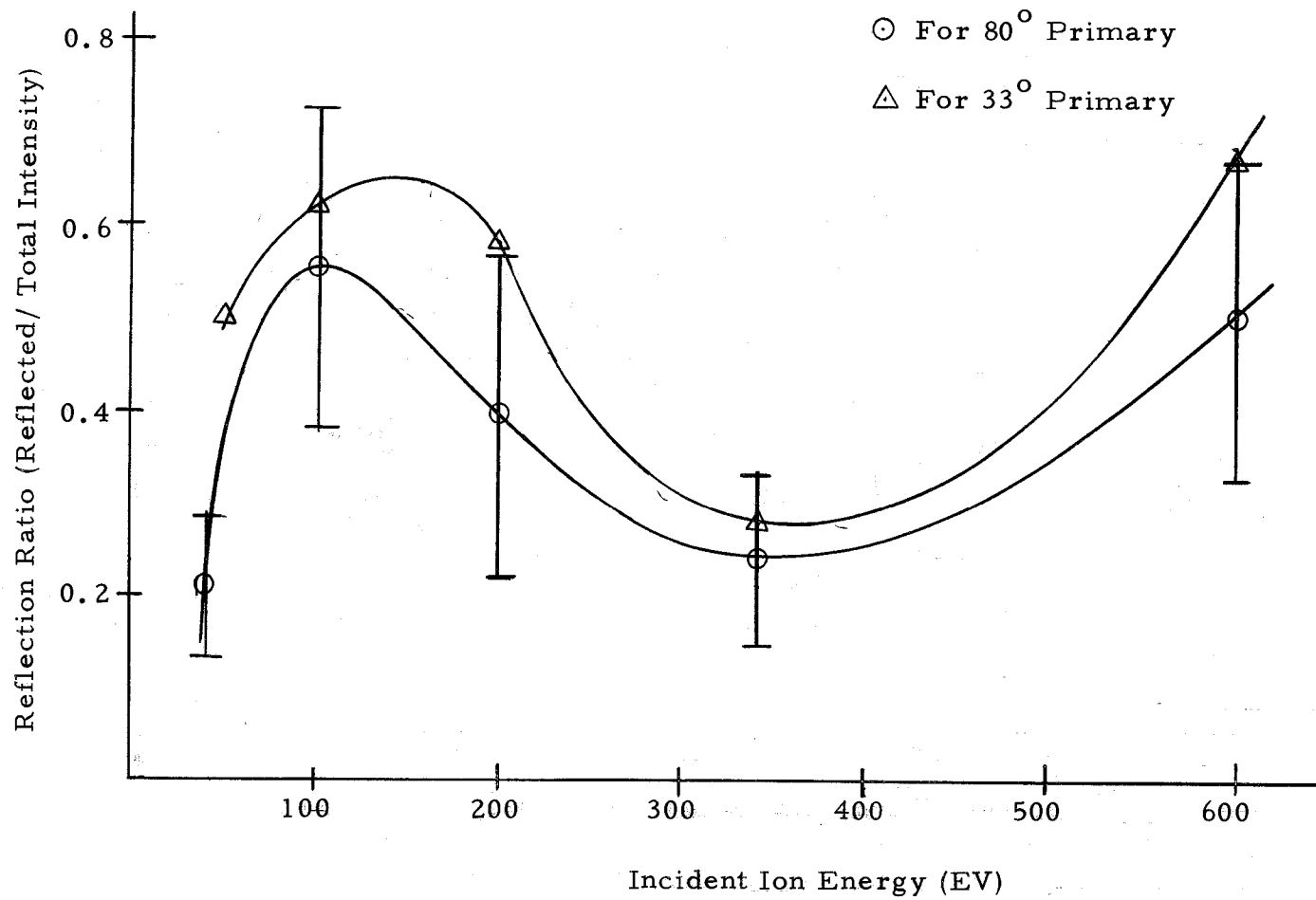
Figure 19. Reflection ratio of sputtered nickel atoms from the molybdenum
collector as a function of incident argon ion energy.

f. Proposed Explanation of Reflection Data

The form of the reflection ratio curves, Figure 19, suggests

resonance scattering of the incident nickel atoms from the interaction

potential that they encounter at the surface. Extrapolating the energy

distribution of sputtered copper atoms to the case of nickel supports

this picture. The requirement for resonance scattering stated by

Schiff (1955, p. 113) is that "an incident particle that has nearly the

right energy to be bound by the potential tends to concentrate there

and produce a large distortion in the wave function and hence a large

amount of scattering." The maximum of the energy distribution of

the nickel atoms would appear, on very good evidence, to occur at an

energy of 1 ev to 2 ev, corresponding to the expected binding energy

of a nickel atom on molybdenum--even allowing for possible lowering

of the binding energy due to gas adsorption. Thus, the condition for

resonance reflection or scattering appears to be fulfilled.

This model would predict a very small energy loss on reflec-

tion--yet enough loss in energy would probably take place to "spoil"

the chance of a second order reflection. Because the energy loss

would be small, specular reflection would occur. The fact that very

little broadening in the reflected atom distribution occurred indicates

that only those nickel atoms reflected which struck the collector at

essentially normal incidence. This is perhaps not unreasonable since

the potential that sputtered atoms see at the molybdenum surface would probably depend on the angle of incidence.

If resonance scattering occurs for some energy E_o, corresponding to a deBroglie wavelength λ_o, it is reasonable to expect that it would also occur for $\lambda = \lambda_o/n$, or $E = nE_o$.

Using this assumption and referring to Figure 20, which shows Stuart and Wehner's energy distribution of sputtered copper atoms from a [110] direction, it is possible to qualitatively explain the shape of the reflection ratio curve.

Let us assume that the distribution of sputtered atoms for nickel bombarded by argon ions is similar to that of Figure 20 and that atoms having this kind of distribution impinge on a metal collector. Let us further assume that resonance scattering occurs at E_o, $2E_o$, ...nE_o, over energy regions $E_n \pm \Delta E$, such that in the limit of large bombarding ion energies, the reflection ratio will be 0.5; this is the order of magnitude of the observed reflection ratios. Choosing the allowed energy regions for scattering, such that they cover roughly 50 percent of the area under the curve for the higher energy curves, yields 0.5 for the reflection ratio as n becomes large. For a given ion bombarding energy, the total area under the curve is proportional to the total number of sputtered atoms; the shaded areas represent sputtered atoms that have the "right" energies to suffer reflection.
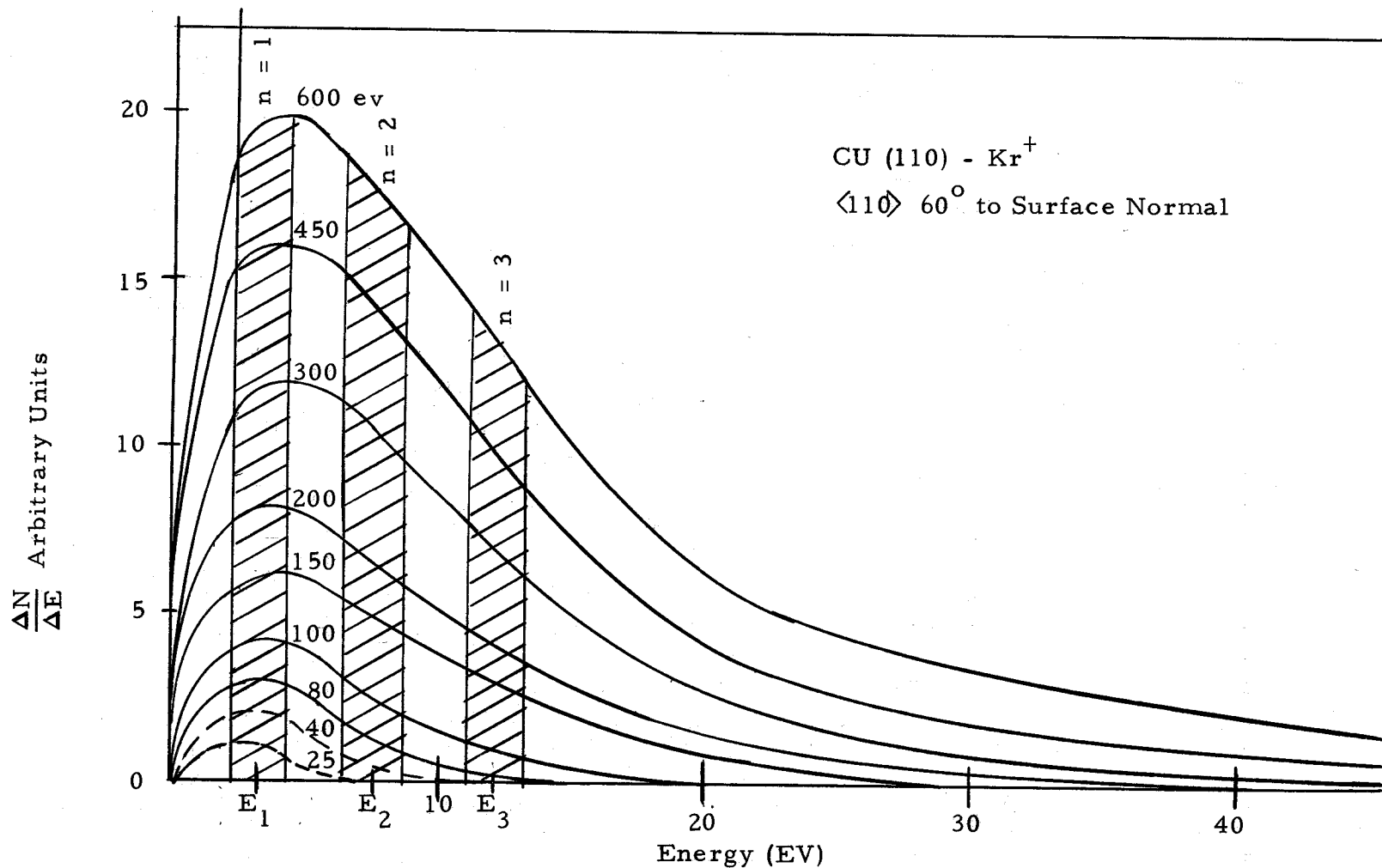
Figure 20. Energy distribution of atoms ejected in the $\langle 110 \rangle$ directions inclined at 60° to the (110) surface normal for bombarding ion energies from 80-600 ev (Stuart and Wehner, 1963). (The addition of the cross hatched areas is to illustrate the proposed reflection mechanism).

At low energies, the reflection ratio will be greatly affected, depending on whether zero, one, two, or three allowed reflection bands of width $2\Delta E$ cross the sputtered atom energy distribution. At higher energies, when n becomes large, the addition of another allowed reflection region will make little difference.

A rough measurement of the areas under the 25 ev, 40 ev and 80 ev yield curves resulted in the derived reflection ratio curve shown in Figure 21. As is seen, it agrees qualitatively with Figure 19.

That other investigators have not noted similar specular reflection may be attributable to (1) a faster sputtering rate so that the collector substrate changed very rapidly to one corresponding to the material of the incident particles, thus destroying the conditions for resonance and making the relative amount of reflected material negligible, (2) use of an experimental geometry in which material reflected either deposited undetected on tube elements or was ignored since most sputtering yield measurements are based on loss of weight of the target, (3) fortuitous choice of materials for target and collector in this experiment, or (4) failure of workers studying reflection coefficients to use atomic beams of sufficiently high energy.

The proposed model of resonance scattering seems to satisfactorily explain the reflection data. In fact, allowing for the presence of surface roughness, it is difficult to visualize another
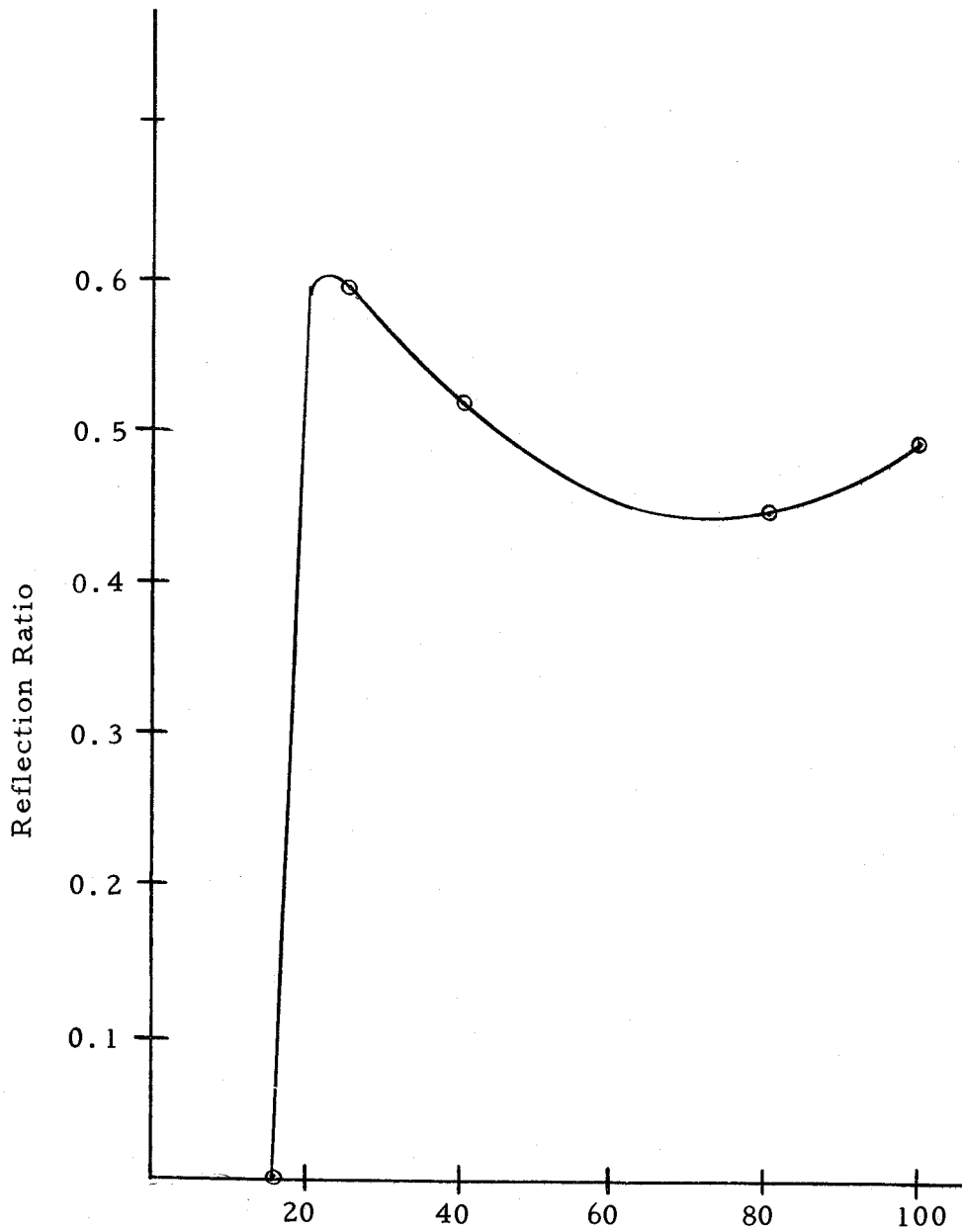
Figure 21. Reflection ratio curve derived from Stuart and Wehner's energy distribution for sputtered copper atoms.

mechanism that would give rise to specular reflection under the pre-
vailing experimental conditions.

G. Discussion of Experimental Errors

a. Introduction

The sources of error in the data were (1) the uncertainty in the
characteristics of the ion beam at final focus, (2) fluctuation of ion
current, (3) non-uniformity in the width of the individual collector
strips, and (4) the statistical error arising from the determination of
the radioactivity distribution on the collector.

b. Uncertainty in Ion Beam Characteristics at Final Focus

Factors contributing to beam energy uncertainty were (1) the
spread of energies occurring in the beam as a result of the ion for-
mation process, (2) the possible presence of contact potentials,
(3) error in determining target potential, and (4) failure to maintain
identical beam focus for all bombardments because of slight varia-
tions in ion chamber pressure and filament current.

Hagstrom (1953) measured the energy distribution of the ions at
final focus, using a parallel plane-electrode retardation chamber.
He found that 98 percent of the ions in the beam had energies within
± 0.4 ev of the mean value.

Measurement of electrode potentials was with respect to the ion

chamber ground potential. An electrolytic tank determination of the

ion chamber equipotentials, in Hagstrom's original design work,

showed that the central portion of the ion beam originated at a 0.9 V

equipotential. This analysis is valid for conditions of low pressure

and small enough electron beam currents to preclude space charge

effects. By measuring the retarding potential between the target and

collector, required to just retard the ions in the beam to zero veloc-

ity at the target, one has a measure of the potential at which ions

form in the ion chamber. For non-space-charge conditions, the

required retarding potential was about 1.0 V, agreeing with the

electrolytic tank prediction. At electron beam currents of about

1 ma, Hagstrom found that the electron space charge depressed the

beam potential by about 5.0 V. As the ion chamber pressure was

increased, the suppressing voltage, for zero ion current to the

target, decreased through zero to a small negative value. He at-

tributes this to ions more-than-neutralizing electron space charge.

Under these conditions, the formation potential of the beam was at

about -0.2 V. The version of Hagstrom's tube used for this experi-

ment, operated at an ion chamber pressure of 5×10^{-5} torr, with a

0.2 ma electron current, and having the target and collector at the

same potential, produced an ion current of about 10^{-11} amp at the

target. This indicates that the beam formation potential must have

been very close to the value predicted from Hagstrom's data, i. e. , a few tenths of a volt negative.

The use of tantalum electrodes throughout the tube presumably eliminated contact potentials except between the tantalum electrode slit at the entrance of the collector and the nickel target. Since the respective work functions of tantalum and nickel are 4. 2 ev and 4. 6 ev, this means that the beam energy is depressed by 0. 4 ev, at this point, thus largely canceling the effect of a slightly negative formation potential for the ions. On the basis of these observations, the value of the ion energy was probably within an electron-volt of the measured value.

The voltage divider voltmeter permitted only rough settings of electrode potentials. The smallest divisions were 5 V for a 250 V full scale reading and 50 V for a 2500 V full scale reading. Measurement of the target potential with a Weston voltmeter allowed voltage measurement to within $\pm$ 0. 5 V on the 40 V scale and $\pm$ 5 V on the 800 V scale; this is based on using one-half of the smallest scale division as the probable error.

One would expect some error to occur as a result of failure to maintain the same beam conditions at the target from one run to the next. It was found that changing the ion current, from one run to the next, produced large scatter in yield curve data points. It appears, largely on the basis of consistency of the data, that using the same

ion current (5×10^{-10} amp) for all runs ensured substantially identical beam distribution at the target.

In summary, it appears that the value of the ion beam energy was within 1 ev or 2 ev, at most, of the measured value, at bombarding energies of 100 ev or less, and that the energy spread in the beam was probably less than 0.5 ev at half maximum intensity.

c. Fluctuation in Ion Current

The main source of ion current fluctuation was the use of the Edison Cell battery power supply for the ion chamber filament. This resulted in a uniform decrease of electron current during the course of a bombardment. Controlling the target current consisted of setting the electrode potentials so that with a 0.2 ma ion chamber electron current, an initial ion current of 5.5×10^{-10} amp resulted at the target. The current was allowed to decrease to 4.5×10^{-10} amp and was then returned to 4.5×10^{-10} amp by increasing the ion chamber filament voltage to restore the initial 0.2 ma electron beam current. Repetition of this sequence several times during the course of a bombardment thus yielded an average ion current of 5×10^{-10} amp. Operation of the Kiethley electrometer in the 10^{-10} amp range permitted current readings to an accuracy of $\pm 0.1 \times 10^{-10}$ amp. Thus, assuming an error of this magnitude, at each end of the range through which the current drifted, yields an average value of current

of $5 \times 10^{-10} \pm 0.2 \times 10^{-10}$ amp.

The initial current adjustment, before starting the timer for a bombardment, typically required about 20 sec. Since the number of ions striking the target in a typical bombardment time of 1000 sec was proportional to the product of the ion current and the time, the fractional uncertainty in the number of ions striking the target ($\frac{\Delta n}{n} = \frac{\Delta i}{i} + \frac{\Delta t}{t}$) was about 0.06. It is noted that the use of a well regulated low voltage D. C. power supply would have improved this by only ± 0.02.

d. Non-Uniformity in the Width of Cut Collector Strips

The use of an indexed fixture, fastened to a shop shear, permitted relatively precise cutting of the collector foil. The resulting strips measured 0.125 ± 0.005 in. Drawing of the best smooth curve through data points presumably averaged out scatter of data due to non-uniform collector strip width.

e. Statistical Error Arising in G-M Counter Analysis

A background count of 850 counts per hour (cph) resulted with the G-M tube enclosed in the lead doghouse. Long count times for background measurements made the error in background negligible compared to the standard deviation error for the total count. Thus the standard deviation, σ_d, for the net count was approximately

$\pm \sqrt{n_t}$, where n_t was the total activity, including background, for a given data point. According to Bleuler and Goldsmith (1960),

$$\sigma_d^2 = \sigma_T^2 \left(\frac{t_d}{t_t}\right)^2 + \sigma_b^2 \left(\frac{t_d}{t_b}\right)^2 ,$$

where σ_t and σ_b are the respective standard deviations of the total count and the background count, and t_d, t_t, and t_b are the respective difference, total, and background count times. Thus, for $t_d = t_t$ and $t_b >> t_d$, $\sigma_d \approx \sigma_t$.

For a count rate of n cph above background, one has for the fractional error in the net count, based on the standard deviation error

$$f = \frac{\sqrt{(n + 850) t}}{nt} , \text{ where } t \text{ is the count time in hours.}$$

For count rates of 50 cph, 250 cph, and 500 cph above background, the required respective count times for ten percent fractional error are 36 hr, 2 hr, and 0.5 hr. It should be noted that these are the count times for each strip of the particular collector being analyzed. Since each collector foil consists of 20 strips, this means that to obtain ten percent statistics for the 25 ev run would require 30 days of continuous counting!

Because the composite peaks consisted of the sum of the net reflected, r, and net primary, p, maximum intensities, the standard deviation fractional error was

$$\frac{\Delta m}{m} = \frac{\sqrt{r + p + 1700}}{r + p} \quad .$$

Since each of the count rates, r and p, derives from a 1 hr count rate

less background, the background count for two hours adds to r and p

to give the total count rate for determining the standard deviation.

The error bars on the data points on the 80° yield curve in Figure 17

indicate the results of this error analysis.

The reflection ratios plotted in Figure 19 are given by

$$R = \frac{r}{r + p}$$

where r and p are as defined above. The indeterminate fractional

error follows from

$$\frac{\Delta R}{R} = \left| \frac{1}{R} \left(\frac{\partial R}{\partial r} \right) \Delta r \right| + \left| \frac{1}{R} \left(\frac{\partial R}{\partial p} \right) \Delta p \right| \quad .$$

Working out the arithmetic results in

$$\frac{\Delta R}{R} = \frac{p \Delta r + r \Delta p}{r(r + p)}$$

where Δr and Δp are $\pm \sqrt{r + 850}$ and $\pm \sqrt{p + 850}$, respectively. The

error bars, thus calculated and plotted on Figure 19, for the 80°

ratios, indicate that the statistics are sufficiently good to establish,

without ambiguity, the shape of the reflection ratio curves.

It is of interest to check the effect of the six percent uncer-

tainty in the number of ions hitting the target during a bombardment,

to see how it affects the final count rate. Replacing $(r + p)$, in the

composite-count fractional error equation by $(1 \pm 0.06)(r + p)$ yields

$$f = \pm \frac{\sqrt{[(r + p)(1 \pm 0.06) + 1700]t}}{(r + p)(1 \pm 0.06)t} .$$

Even for count rates of 500 cph, it is seen that the effect on the final

error is only of the order of one percent. Thus, the limiting factor

in the experiment was the length of counting time allotted per col-

lector foil.

V. SPUTTERING THEORY

A. Types of Theoretical Approaches

The literature cites two of the various theoretical explanations of sputtering most frequently. They are (1) the thermal-spike evaporation theory proposed by von Hippel (1926) and more recently extended by Townes (1944), and (2) the momentum-transfer, radiation-damage theory.

The evaporation theory assumes that the collision of an incident ion with a solid raises the temperature of a small local region of atomic dimensions above the sublimation energy of the atoms on the target surface. According to this model, the evaporated atom carries away some of the energy of the resulting thermal spike. The remainder rapidly dissipates in the solid by thermal conduction. Thus, the only parameters involved are the energy of the incident ion, the sublimation energy of the sputtered material, and the thermal conductivity of the target. According to this theory, the sputtering yield should be independent of the angle of incidence and of the masses of the target and incident atoms. Overwhelming evidence from sputtering of single crystals indicates that the sputtering yield is a function of both angle of incidence and of the respective masses of the interacting particles. To date, the evaporation theory has been unable to provide an estimate of sputtering thresholds.

Because the evaporation or thermal spike theories have been completely unsuccessful, the balance of this discussion will deal with the radiation-damage, momentum-transfer approach to sputtering.

B. Momentum Transfer Theories

a. General Approach

All current momentum-transfer theories assume that sputtering results from one or more binary collisions (in a binary collision, the interaction between any two particles is completed before either of them interacts with a third particle). Most of the theoretical efforts in the literature assume a free particle lattice, thereby neglecting the effect of lattice binding. A common characteristic of all sputtering theories is that they all require the use of lattice parameters which have not yet been accurately determined.

Preferential sputtering from close-packed directions of a crystal requires a theory which incorporates crystal structure. The approach here has been to look at how energy released in a crystal dissipates, to determine what kinds of interactions occur in the energy range of interest, and to extrapolate the bulk behavior to the surface, since everyone assumes sputtering is a surface phenomenon. Silsbee (1957) showed that if a particle hits a row of atoms in a close packed direction with a very small component of transverse

momentum (a not-quite head-on collision), the angular displacement of each successive atom in the row becomes smaller, and momentum propagates along the row, or chain, until it encounters a vacancy or lattice defect. In fcc metals, Silsbee predicts focussing only in $\langle 110 \rangle$ directions. Gibson et al. (1960) did a computer calculation to find out how momentum, incident onto a copper lattice, dissipates. They assumed pair-wise interaction and energy loss from a chain by interaction with neighboring chains. Their results show focussing can also occur in $\langle 100 \rangle$ and $\langle 111 \rangle$ directions.

For most gas ions impinging on metals, the ion energy required to significantly penetrate the electron shells of the target atoms is of the order of 1 kev to 10 kev. On this basis, low energy sputtering seems to be a hard sphere collision process.

Of the low energy sputtering theories, those by Langberg (1958) and Henschke (1957) are most often cited in conjunction with poly-crystalline sputtering. They begin with somewhat different initial assumptions. Langberg assumes that an ion strikes a surface atom in a non-head-on collision, causing it to rebound against a neighboring surface atom which then sputters. Henschke assumes several mechanisms. At oblique incidence, he proposes that an ion can directly sputter a surface atom; at normal incidence he requires that the ion penetrates into the lattice, rebounds from a lower atomic plane and finally sputters a surface atom. Langberg assumes a

Morse potential between lattice atoms while Henschke assumes

billiard ball collisions. Henschke proposes an energy transfer model

based on the theory of collisions with restitution, but assumes a

lattice interaction loss-coefficient for impulse. Langberg conserves

both energy and momentum, then corrects for energy loss to the

lattice by making a perturbation calculation.

The predictions of the two theories are similar. However,

Langberg's, because of simpler assumptions, contains fewer un-

determined lattice parameters. In addition, it appears in a form

which is much more amenable to comparison with experiment. Both

theories calculate yields for the threshold and linear regions of the

yield curve, such as Figure 17, not on the basis of their sputtering

models but in terms of probability arguments. This permits fitting

theoretical yield curves to experimental data by choosing a suitable

value for one or more arbitrary constants.

Harrison and Magnuson (1961) have made the only attempt, to

date, to explain preferential sputtering in close packed directions as

a function of crystal structure. Unfortunately, their work is limited

to calculating the sputtering threshold and says nothing about sputter-

ing yields from different crystallographic directions. It should be

pointed out that their theory is of particular interest because the

present experimental study permits, for the first time, a direct

comparison of an experimental directional threshold value with a

theoretical prediction based on the Silsbee chain mechanism.

Harrison (1956) applied the methods of neutron diffusion theory to explain the form of the sputtering yield curve at energies in the middle of the linear region and above. However, this theory is very sensitive to the choice of poorly determined lattice coefficients. The values fitted to his theory brings it into fair agreement with poly-crystalline yield curves. It would seem, on the basis of the early saturation of the yield curves in the present experiment and in the Strayer, Cooper, and Swanson data, that such agreement does not go very far toward explaining the mechanism of sputtering.

Thus, a general review of sputtering theory reveals that no satisfactory model exists to explain the shape of the sputtering yield curve, but that several explanations of the sputtering threshold exist. The subsequent sections will present the Langberg and Harrison-Magnuson theories, and compare the predictions with the experi-mentally measured values.

b. The Langberg Theory of Sputtering

As stated in section a., Langberg assumed (1) a two-binary-collision process to explain sputtering, (2) a Morse potential be-tween lattice atoms, and (3) that the minimum energy required for sputtering depends on the number of surface bonds, and the energy lost to the lattice.

The Morse potential is given by

$$U(r) = \phi \left\{ \exp \left[a(d - r) \right] - 1 \right\}^2$$

where ϕ is the energy required to break a bond, a is a lattice parameter related to compressibility and d is the equilibrium displacement.

Calculation of the energy transferred by an ion to a surface atom, for an arbitrary recoil angle, permits maximizing the energy transferred to a sputtered surface atom. Correction for energy loss to the lattice, which turns out to be about ten percent, and determining the number of bonds per surface atom then allows the calculation of the minimum threshold energy. The sum of the energy to free the first surface atom and the energy required to sputter the second surface atom yields the expression for the sputtering threshold energy.

Assuming, with Langberg, that a particle of mass M and energy E_o impinges onto the surface at normal incidence but strikes a surface atom of mass m_1 in a non-head-on, elastic collision permits the calculation of the recoil energy as a function of the recoil angle, θ_1, of m_1. The result is

$$E_1 = T_{m_1} E_o \cos^2 \theta_1, \text{ where } T_{m_1} = 4Mm_1 / (M + m_1)^2$$

and E_1 is the recoil energy of m_1.

If, then, m_1 collides elastically, at an angle of incidence θ_1, with m_2 (the atom which sputters), the potential energy stored in the second collision is

$$U(R) = \frac{m_2}{m_1 + m_2}\left(T_{m_1} E_o \cos^2\theta_1\right)\left(1 - \frac{d^2 \cos^2\theta_1}{R^2}\right).$$

In the above equation, R is the hard sphere collision radius and d is the lattice spacing. Taking $\dfrac{\partial U(R)}{\partial \cos^2\theta_1} = 0$ optimizes the energy transfer condition with respect to recoil angle. This results in

$$U(R)_{Max} = \overline{U}(R) = m_2 T_{m_1} E_o R^2 / 4(m_1 + m_2) d^2.$$

The value of $\cos^2\theta_1$, for which $U(R) = \overline{U}(R)$, is given by

$$(\cos^2\theta_1)' = R^2 / 2d^2.$$

Langberg states that the kinetic energy acquired by m_2 under optimum conditions is

$$K_2 = 2\overline{U}(R)m_1 / \gamma(m_1 + m_2),$$

where γ depends on $U(r)$ and for low energy sputtering is a constant having a value of approximately 0.63.

To account for binding, Langberg assumes that, on the average, N bonds of binding energy ϕ hold a surface atom in place. But, it is noted, some energy loss to neighboring lattice atoms also occurs during the collision process. Thus, the binding energy of

m_2 is effectively somewhat increased. It is given by $E_B = \sigma N\phi$,

where σ is approximately 1.1 (obtained from a perturbation calcula-

tion).

Noting that the sublimation energy, H, for a surface atom, is

$H = n\phi/2$, where n is the number of nearest neighbors, and setting

$K_2(min) = \sigma N\phi = 2H\sigma N/n$

$$\frac{2H\sigma N}{n} = 2\overline{U}(R)m_1/\gamma(m_1 + m_2).$$

Substituting the expression for $\overline{U}(R)$ in the above equation and solving

for $E_o = E'$, which is the minimum energy required to sputter m_2,

gives

$$E' = 16HNd^2 \gamma\sigma / nT_{m_1} T_{m_2} R^2,$$

where $T_{m_2} = 4m_1 m_2/(m_1 + m_2)^2$. However, energy is also required

to break m_1 free from its lattice site. This energy is given by

$$E'' = H/T_{m_1} Cos^2 \theta_1 = 2Hd^2/T_{m_1} R^2.$$

Thus, the threshold energy, E_N, for sputtering is

$$E_N = E' + E''.$$

Substituting the Morse potential U(R) for $\overline{U}(R)$ into $K_2(min) =$

$2\overline{U}(R)m_1/\gamma(m_1 + m_2) = 2H\sigma N/n$ allows one to solve for R/d. Putting

the resulting value of R/d into E' and E'' yields, for the case of

$m_1 = m_2$,

$$E_N = \frac{10H}{T_{m_1}} \left(\frac{1.1N}{n} + 0.2 \right) \left[1 - \frac{1}{ad} \ln (1 + 0.83N^{1/2}) \right]^{-2}.$$

If one designates N_A and N_B as the respective maximum and minimum numbers of surface bonds, $N_A = 9$ and $N_B = 4$ for sputtering from a (100) plane of a fcc crystal. In this instance, there are 12 nearest neighbors. For nickel, Langberg states that $H = 4.413$ ev and $ad = 3.582$.

In order to determine the sputtering yield, Langberg assumes for $E_A \leqslant E \leqslant E_B$ that $S_N = \Sigma P(E)(E - E_N) dE_N$, where E_N is the threshold energy for an atom with N bonds, $S(N)$ is the sputtering yield, and $P(E)$ is the probability of sputtering an atom, by an ion of energy E. Evaluating, for $N_A \leqslant N \leqslant N_B$ or $E_A \leqslant E \leqslant E_B$, where $E_A = \sigma \phi N_A$ and $E_B = \sigma \phi N_B$, yields, in the limit, if one assumes $P(E) = b = $ a constant,

$$S = \int_{E_B}^{E_A} b(E - E_n) dE_n.$$

On carrying out the integration,

$$S = \frac{b}{2} (E - E_N)^2 \quad \text{for } E_A \leqslant E \leqslant E_B.$$

For $E > E_A$ all ions can sputter surface atoms having the strongest bonds (E_A). If one takes $dE_N = (E_A - E_B)$ and $E_N = (1/2)(E_A + E_B)$,

$S = (b/2)(2E - E_A - E_B)(E_A - E_B)$ for $E > E_A$.

The data of Zdanuk and Wolsky (1965), for the sputtering of copper by argon ions, near threshold energy, indicates that the yield curve bends very sharply toward the axis, in what could be described as a quadratic behavior, starting at about 50 ev. Their lowest data point was at 20 ev. It is noted that the yield data in the present experiment did not indicate a quadratic approach to threshold for nickel bombarded by argon ions.

c. The Harrison-Magnuson Theory of Sputtering Thresholds

Silsbee (1957) showed that under certain conditions energy or momentum directed onto or released within a crystal "focusses" along directions of closest packing. Figure 22 shows how this can occur. If $D/R \leqslant 2$ (where D is the lattice spacing along a row and R is the impact parameter of the individual atoms of the crystal), then focussing is possible. If a particle strikes a row of close packed atoms, (referred to in the literature as a chain), in a non-head-on collision, the angle that each successive perturbed atom makes with the axis of the row becomes smaller. Thus, some of the momentum of the initial collision becomes directed along the chain. If the impact parameters of the atoms of a chain do not overlap, then the scattering angle which each successive atom of a row makes with the axis of the row becomes larger. In this case, an atom will ultimately scatter out of the chain.
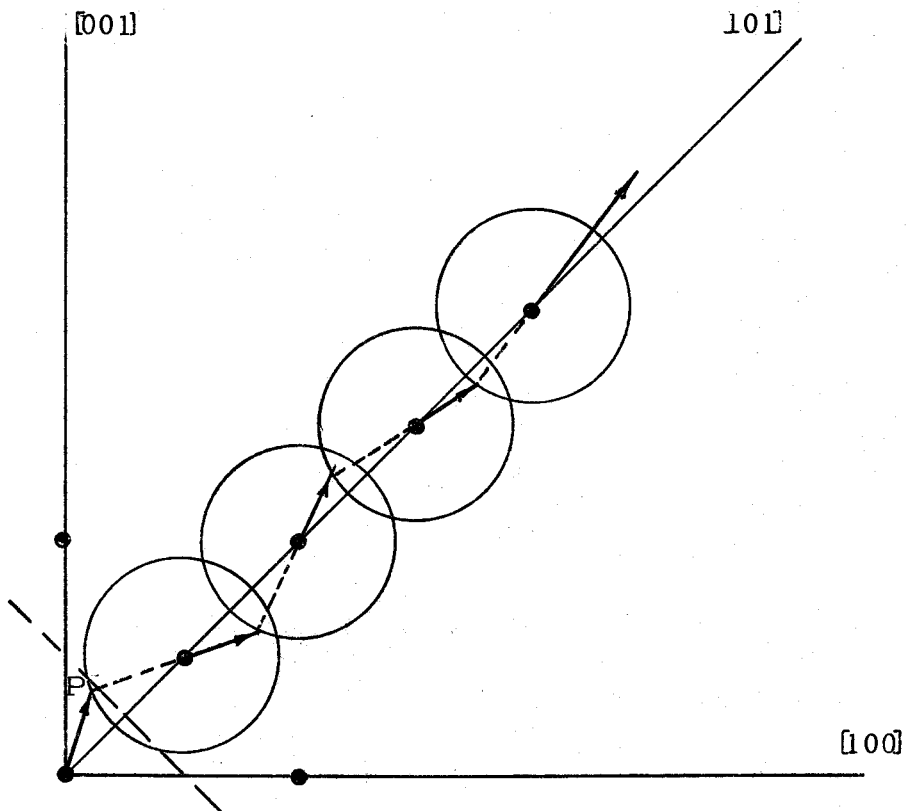
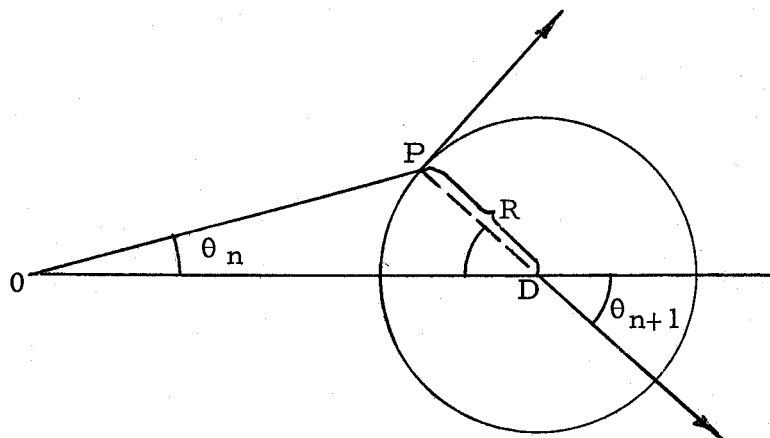Figure 22. Focussing collisions along a [10̄1] direction in a fcc crystal.

Figure 23. Single collision between two hard spheres of radius R/2 showing P as the point of impact.

Figure 23 shows the case for a collision in which two equal

masses, having equal masses and radii, collide elastically at point

P. The relationship between θ_n, the initial angle of incidence, and

θ_{n+1}, the recoil angle of the struck atom, is

$$\text{Sin } \theta_{n+1} = \text{Sin } \theta_n \left[\alpha \text{ Cos } \theta_n - (1 - \alpha^2 \text{Sin}^2 \theta_n)^{1/2} \right],$$

where $\alpha = D/R$. A calculation for the corresponding energy transfer

yields

$$E_{n+1} = E_n (1 - \alpha^2 \text{Sin}^2 \theta_n).$$

In Silsbee's theory, the sole function of the projectile atom is

to impart momentum to a target atom. Once this is done, the pro-

gram is to study how the target atom transfers its recoil energy

along a close packed direction. Harrison and Magnuson assume,

when they apply Silsbee's chain mechanism to sputtering, that the

incident particle becomes oriented along a chain direction and that

the momentum it has when it finally becomes "focussed" can reflect

back along the chain to eject a surface atom. Thus, the approach is

somewhat different than Silsbee's. As a result, it appears some-

what more convenient to develop sputtering theory in center of mass

coordinates and then transform the results back to the laboratory

system.

In the center of mass system one has for a binary, elastic

collision

$$\frac{E_1}{E_o} = (1/2)\left\{ 1 + \left(\frac{M-m}{M+m}\right)^2 + \left[1 - \left(\frac{M-m}{M+m}\right)^2 \right] \cos\phi \right\}$$

where E_o is the energy of the incident ion, E_1 is its energy after

collision, M and m are the respective masses of the ion and target

atoms, and ϕ is the recoil angle in center of mass coordinates.

Simplification of the above relationship yields

$$\frac{E_1}{E_o} = (1 - T_m \sin^2 \phi / 2),$$

where $T_m = 4Mm/(m+M)^2$. Harrison and Magnuson assume that

n equal angle collisions occur before the incident ion becomes re-

oriented in a chain direction. The fraction of its initial energy that

the ion still has after n such collisions is therefore

$$\frac{E_n}{E_o} = \left[1 - T_m \sin^2 \phi / 2 \right]^n = R_n.$$

Thus the amount of energy which is available to reflect back along a

chain and sputter an atom is

$$E_n = E_o R_n.$$

The energy transferred to a target atom in an elastic head-on

collision is $T_m E_o$. Harrison and Magnuson (1961, p. 1424) state,

"All impacts which exceed the maximum impact parameter are

actually smaller angle impacts upon another atom." From this,

they conclude that most of the ion-atom collisions are small angle collisions, and, thus, the energy transmitted to a chain approximately equals that which would result in a head-on collision. Since the ion rebounds from the surface and does not make further collisions with the lattice, it suffices to take $n = 1$ for the number of collisions required to re-orient the incident particle in a chain direction. Thus, the energy available for sputtering is $R_1 T_m E_o$. Setting this expression equal to the surface atom binding energy, H_{hkl}, and solving for the minimum ion energy for sputtering, $E_o = E_t$, yields the sputtering threshold energy

$$E_T \leqslant \frac{H_{hkl}}{T_m} \left[1 - T_m \sin^2\phi/2 \right]^{-1} .$$

Converting to laboratory coordinates, using the transformation

$$\sin^2\phi/2 = (1/2) \left\{ 1 + \mu\sin^2\theta - \cos\theta \left(1 - \mu^2\sin^2\theta \right)^{1/2} \right\} ,$$

yields for the threshold energy

$$E_t = \frac{H_{hkl}}{T_m} \left\{ 1 - (1/2) T_m \left[1 + \mu\sin^2\theta - \cos\theta \left(1 - \mu^2\sin^2\theta \right)^{1/2} \right] \right\}^{-1} .$$

The constant μ is the mass ratio M_{ion}/m_{atom}. If one considers the conditions for sputtering a surface atom at the end of a particular chain, θ is the angle through which incident momentum must be re-oriented so that it focusses out of the surface along the chain.

As was seen in section b., Langberg used the sublimation

energy as a first approximation to the surface binding energy. He

then corrected for the smaller "average" number of bonds which hold

a surface atom in position than is the case for an atom in the interior

of the crystal. Using similar reasoning, Harrison and Magnuson

somewhat arbitrarily assumed that $H_{hkl} = H/5$, where H is the sub-

limation energy.

d. Comparison of Theoretical Predictions with Experimental Results

Evaluating Langberg's threshold expression, given in section

b., yields $50 < E_t < 110$ ev, depending on whether one uses N_A or

N_B in the calculation. The average predicted value is thus about

80 ev.

It is noted that the Harrison-Magnuson theory predicts that the

threshold energy depends on the angle of incidence of the impinging

ions with respect to the directions of closest packing. Figure 17

shows that indeed there seems to be a slight dependence of the

threshold energy on the angle of incidence. However, the shift, as

one goes from the 80° maximum to the -17° maximum is only from

about 18 ev to about 25 ev. The respective scattering angles, θ, for

use in evaluating the Harrison-Magnuson formula, for the 80° chains

and the -17° chains are 105° and 165°. Substituting these values into

the formula yields threshold values of 10 ev and 90 ev, respectively.

It is seen that the latter prediction compares closely with the results from Langberg's formula for normal incidence. This is perhaps not surprising since the chain contributing the -17° maxima is not too far from the surface normal, and the basic assumptions of the two theories are actually quite similar.

The fact that the 18 ev measured threshold for 80° is of the same order of magnitude as the Harrison-Magnuson 10 ev prediction appears purely coincidental since the -17° values are in such complete disagreement.

Thus, it is seen that neither the Harrison-Magnuson nor the Langberg theory successfully explains sputtering threshold behavior. The main difficulty, it is proposed, is that present theories all assume a purely surface interaction. The fact that the threshold, for a given chain, shows only a very small dependence on the angle of ion incidence indicates that the crystal lattice is much more involved in the process than previously believed. It appears as though once energy is released in a crystal, it loses its sense of direction and becomes distributed equally, or almost so, in the directions of closest packing. This kind of a model would explain why almost the same threshold value appears for 80° as for -17°. The assumption of the hard-sphere, surface interaction seems to provide too inefficient an energy transfer mechanism between the impinging ions and the ejected surface atoms, particularly at normal or near

normal incidence, for the Harrison-Magnuson theory; the same

difficulty also occurs in Langberg's normal incidence model. In

addition, the pair-wise interaction, assumed in all the theories pro-

posed to date, may be an oversimplification.

Because of the departure of the experimental yield curves

from previously observed polycrystalline or "whole plane" yields, it

does not seem meaningful to compare the measured yield curves

with those predicted by Harrison's (1956) "neutron diffusion" theory,

Langberg's statistical model, or other approaches which have been

"fitted" to previous experimental results.

VI. CONCLUSIONS

The results of the experimental program may be summarized as follows:

(1) The "single direction" yield curves saturate much sooner, with increasing ion energy, than do either the polycrystalline or "whole plane" yields.

(2) The polycrystalline and "whole plane" yields can be explained as the superposition of yields from the directions of closest packing and yields from the directions of next closest packing.

(3) On the basis of the explanation of polycrystalline and "whole plane" yield curves, it appears that the sputtering thresholds occur at much higher energies for the next closest packed directions than for the directions of closest packing.

(4) The sputtering thresholds for the $\langle 110 \rangle$ directions of nickel, at 80° and -17° with respect to the incident beam, are about 18 ev and 25 ev, respectively. Comparison of the yield curves with polycrystalline data indicates that the "second threshold" (for sputtering from $\langle 100 \rangle$ directions) must be of the order of 50 ev to 100 ev.

(5) The "saturation yield" appears to be a much more sensitive function of the angle of incidence, with respect to the ejection direction, than is the threshold energy for sputtering.

(6) The experimental observation of specular reflection of nickel from molybdenum appears explainable as resonance scattering from the interaction potential that the nickel atoms encounter at the molybdenum surface.

(7) No successful theory of sputtering presently exists; the detailed picture of sputtering from a single direction, which this experimental study produced, should provide the basis for a new and, hopefully, more successful theoretical approach.

BIBLIOGRAPHY

1. Anderson, C. S. Atom ejection in low energy sputtering of single crystals of fcc metals and of Ge and Si. Journal of Applied Physics 33:2017-2025. June 1962.

2. Bleuler, Ernst and George J. Goldsmith. Experimental nucleonics. New York, Holt, Rinehart and Winston, 1960. 393 p.

3. Cabrera, N. The structure of crystal surfaces. Discussions of the Faraday Society 28:16-22. 1959.

4. Creighton, H. J. and W. A. Koehler. Principles and applications of electrochemistry. 2d ed. Vol. 2. New York, Wiley, 1944. 573 p.

5. Germer, Lester H. The structure of crystal surfaces. Scientific American 212:32-41. March 1965.

6. Gibson, J. B. et al. Dynamics of radiation damage. Physical Review 120:1229-1253. Nov. 1960.

7. Guy, Albert G. Elements of physical metallurgy. 2d ed. Reading, Massachusetts, Addison-Wesley, 1960. 528 p.

8. Hagstrom, Homer D. Instrumentation and experimental procedure for studies of electron ejection by ions and ionization by electron impact. Review of Scientific Instruments 24:1122-1142. Dec. 1953.

9. Harrison, D. E. Theory of the sputtering process. Physical Review 102:1473-1480. June 1956.

10. Harrison, D. E. and G. D. Magnuson. Sputtering thresholds. Physical Review 122:1421-1430. June 1961.

11. Henschke, E. B. Collision theory of cathode sputtering. Physical Review 106:737-753. May 1957.

12. Hirth, J. P. and G. M. Pound. Condensation and evaporation (nucleation and growth kinetics). Progress in Materials Science 11:1-14. 1963.

13. Kay, Eric. Impact evaporation and thin film growth in a glow discharge. Advances in Electronics and Electron Physics 17:245-322. 1962.

14. Koedam, M. Cathode sputtering by rare-gas ions of low energy. Philips Research Reports (Netherlands) 16:101-144, 266-300. 1961.

15. Laegreid, Nils and G. K. Wehner. Sputtering yields of metals for Ar^+ and Ne^+ ions with energies from 50 to 600 ev. Journal of Applied Physics 32:365-369. March 1961.

16. Langberg, Edwin. Analysis of low-energy sputtering. Physical Review 111:91-97. July 1958.

17. Mac Rae, A. U. Absorption of oxygen on the (111) (100) and (110) surfaces of clean nickel. Surface Science 1:319-348. 1964.

18. Schiff, Leonard I. Quantum mechanics. 2d ed. New York, McGraw-Hill, 1955. 417 p.

19. Silsbee, R. H. Focusing in collision problems in solids. Journal of Applied Physics 28:1246-1250. Nov. 1957.

20. Strayer, R. W., E. C. Cooper and L. W. Swanson. Field emission and ion microscopy investigation of the sputtering of tungsten by cesium and xenon. Paper read at the 25th Annual Conference on Physical Electrons, Massachusetts Institute of Technology, Cambridge, Mass., March 1965.

21. Stuart, R. V. and G. K. Wehner. Energy distribution of sputtered Cu atoms. Journal of Applied Physics 35:1819-1824. June 1964.

22. Townes, Charles H. Theory of cathode sputtering in low voltage gaseous discharges. Physical Review 65:319-327. June 1944.

23. U. S. Oak Ridge National Laboratory. Catalog-radio and stable isotopes. Oak Ridge, Tennessee, 1963. 99 p.

24. von Goeler, E. and E. Lüscher. Absorption study of gold atoms on molybdenum. In: Proceedings of the Fifth International Conference on Ionization Phenomena in Gases, Munich, 1961. Amsterdam, North-Holland, 1962. p. 161.

25. von Goeler E. and R. N. Peacock. Radiotracer measurement of the desorption energy of silver from molybdenum and nickel. Journal of Chemical Physics 39:169-174. July 1963.

26. von Hippel, Artur. Zur Theorie der Kathodenzerstäubung. Annalen der Physik 81:1043-1075. 1926.

27. Wehner, G. K. Sputtering by ion bombardment. Advances in Electronics and Electron Physics 7:239-298. 1955.

28. _____. Controlled sputtering of metals by low-energy Hg ions. Physical Review 102:690-704. May 1956.

29. _____. Physical sputtering. In: Proceedings of the Fifth International Conference on Ionization Phenomena in Gases, Munich, 1961. Amsterdam, North-Holland, 1962. p. 1141-1156.

30. Zdanuk, E. J. and S. P. Wolsky. Sputtering of single-crystal copper and aluminum with 20-600 ev argon ions. Journal of Applied Physics 36:1683-1687. May 1965.

31. Zwanzig, R. W. Collision of a gas atom with a cold surface. Journal of Chemical Physics 32:1173-1177. April 1960.